

Estimating the coherence of noise in mid-scale quantum systems

Pedro Figueroa-Romero¹, Miha Papič^{1,2}, Adrian Auer¹, and Inés de Vega^{1,2}

¹IQM Quantum Computers, Georg-Brauchle-Ring 23-25, 80992 Munich, Germany

²Department of Physics and Arnold Sommerfeld Center for Theoretical Physics, Ludwig-Maximilians-Universität München, Theresienstr. 37, 80333 Munich, Germany

While the power of quantum computers is commonly acknowledged to rise exponentially, it is often overlooked that the complexity of quantum noise mechanisms generally grows much faster. In particular, quantifying whether the instructions on a quantum processor are close to being unitary has important consequences concerning error rates, e.g., for the confidence in their estimation, the ability to mitigate them efficiently, or their relation to fault-tolerance thresholds in error correction. However, the complexity of estimating the coherence, or unitarity, of noise generally scales exponentially in system size. Here, we obtain an upper bound on the average unitarity of Pauli noise and develop a protocol allowing us to estimate the average unitarity of operations in a digital quantum device efficiently and feasibly for mid-size quantum systems. We demonstrate our results through both experimental execution on IQM SparkTM, a 5-qubit superconducting quantum computer, and in simulation with up to 10 qubits, discussing the prospects for extending our technique to arbitrary scales.

The main obstacle for quantum computing undeniably remains the presence of noise, causing a multitude of errors that limit the usefulness of currently available quantum processors. That is to say, not all quantum noise is made equal, and ironically, figures of merit that are efficient to access in an experiment –such as the fidelity of a quantum operation– are often by definition insensitive to many of the details of such noise. It is thus imperative to have a plethora of protocols

with certain practical desiderata that can probe different aspects of noise, and that can then, in turn, provide actionable information to existing methods to suppress, mitigate, or fully correct potential errors.

Quantum noise can be described as an undesirable quantum transformation mapping the ideal noiseless output state of a quantum computation into some other valid, albeit unexpected, output quantum state. Focusing on the regime where such noise is *effectively* Markovian, i.e., it only depends on the input state and no other external context variables, a comprehensive classification of all possible errors can be made [1], but in particular it is extremely important to be able to distinguish between *coherent* and *incoherent* error contributions.

Coherent noise can be described as a deterministic, undesired unitary transformation, e.g., it can arise due to imperfect control or calibration of quantum gates, and also due to certain types of crosstalk [2]. Incoherent or stochastic noise, on the other hand, is described by non-unitary transformations and arises purely statistically, e.g., a bit-flip occurring with a certain non-zero probability, or so-called *depolarizing noise*, whereby a state gets maximally mixed with a certain probability but remains intact with the complementary probability. Generally, Markovian quantum noise will be described by a quantum operation that contains both coherent and stochastic noise contributions. The reasons why distinguishing between these is important, include:

- i*) Coherent errors can, for example, be effectively suppressed by good experimental quantum control, while incoherent errors in isolation can be efficiently mitigated [3–7] and fully corrected [8, 9].

Pedro Figueroa-Romero: pedro.romero@meetiqm.com

- ii) Coherent errors can accumulate in a much more detrimental way and provide error-rate estimates, such as average gate-fidelity, that can differ by orders of magnitude from worst-case estimates (i.e., fault-tolerance thresholds) [10–14].
- iii) The interpretation of average gate fidelity as a reliable and meaningful error rate depends heavily on the noise having a low coherent contribution [12, 15–17].

The average coherence of a noisy quantum gate can be understood as a measurement of the rate at which noise shrinks the n -dimensional Bloch ball, as depicted in Fig. 1, and can be measured by its *unitarity*, which in turn can be estimated operationally by Unitarity Randomized Benchmarking (URB) [12]. Despite being efficient and robust to State Preparation and Measurement (SPAM) errors, URB is not scalable in system size, as it requires estimating an exponential amount of expectation values within a Randomized Benchmarking (RB)-like protocol. The reason for this is not URB *per se*, but rather that fundamentally, the unitarity is a second-order functional of the noise, akin to the case of the so-called *purity* for a quantum state.

In general, the complexity of characterizing quantum noise comprehensively typically scales exponentially with system size [18, 19]. Even the most efficient of protocols estimating a single figure of merit, such as those within the family of RB [20], fail to do so at scale. However, with the quantum industry inevitably moving towards larger systems, there is a pressing need to find ways to generalize such tools to larger systems.

Recently, scalable RB-based techniques such as Mirror Randomized Benchmarking (MRB) [21, 22] and Binary Randomized Benchmarking (BiRB) [23], among others [24, 25], have been developed, which can estimate the average fidelity of sets of quantum operations in a scalable, efficient and SPAM-robust way, for a large class of gate sets. On the other hand, Randomized Measurements (RM) techniques, and so-called classical shadows, have enabled the efficient estimation of properties of many-body quantum systems [26, 27] (including state fidelity and purity), linear properties of gate sets [28], and characterization of processes with memory [29].

We harness the results of [30–33], together with

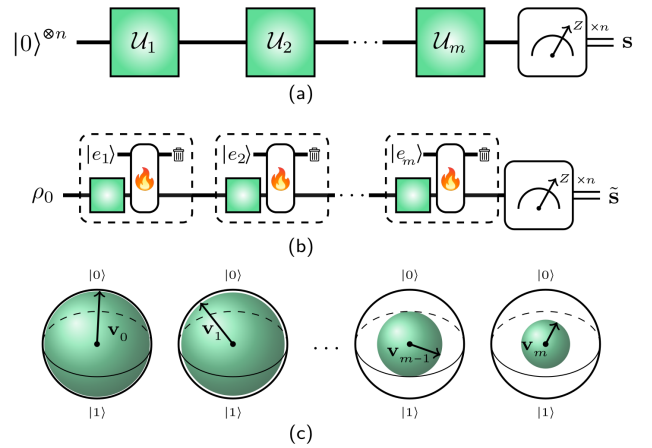


Figure 1: **Coherence of noise and loss of purity:** (a) An ideal quantum computation on n qubits can be described by an initial state $|0\rangle^{\otimes n}$, a sequence of unitary operations U_i , and a computational basis measurement with output $s \in \{0, 1\}^n$. More realistically, in (b), the initial state can be statistically mixed and correlated among qubits, and operations are subject to noise due to interactions with external degrees of freedom $|e_i\rangle$ that further reduce the state purity. In (c), the impurity of each state $\rho_i := \frac{1}{2^n} (\mathbb{1} + \mathbf{v}_i \cdot \mathbf{P})$ after the i^{th} operation, where \mathbf{P} is a vector of all n -qubit Pauli matrices and \cdot an inner product, can be depicted as a shrinkage of the 2^{n-1} -dimensional Bloch vector, $|\mathbf{v}_0| \geq |\mathbf{v}_1| \geq \dots \geq |\mathbf{v}_m|$; such shrinking can be associated on average to the *unitarity* or *coherence* amount of the noise, which is a resource-intensive quantity to characterize experimentally as n increases.

a scalable RB-inspired protocol, to develop a standalone technique allowing to simultaneously estimate the average fidelity and average unitarity of layers of operations in mid-scale quantum systems. Moreover, we first identify an interval for the unitarity of so-called stochastic Pauli noise in terms of average fidelity, enabling certification of whether average noise has a low coherent contribution and establishing meaningful error budgets via the average unitarity.

In § 1 we introduce the main technical background, while in § 2 we present a new upper bound on the unitarity of Pauli noise. In § 3 we summarize existing results regarding RMs, before presenting our protocol in § 4, which in § 5 we demonstrate with experimental execution on IQM SparkTM [34]. In the remaining § 6 we discuss the bottlenecks for a scalable estimation of average coherence of noise, and finally, we draw some conclusions and prospects to overcome mid-scalability in § 7.

1 Average coherence of noise and its relation with purity and fidelity

It is well known that no physical system can be perfectly isolated. In particular, the loss of coherence of quantum states is one of the fundamental practical problems facing any quantum technology. In general, the dissipation of information to an external environment results in an increasingly mixed classical probability distribution over a set of possible quantum states. Such mixedness or uncertainty can be quantified by the purity of the respective density matrix ρ , given by $\text{tr}(\rho^2)$. The purity takes extremal values of 1 for a pure state, and 2^{-n} for a maximally mixed state on n -qubits, and it can also be written as the Schatten 2-norm $\|\rho\|_2^2$, where $\|X\|_2 = [\text{tr}(XX^\dagger)]^{1/2}$.

Logical operations or gates \mathcal{G} in a quantum computer are described by unitary operators, which by definition preserve the purity of quantum states, i.e., for $\mathcal{G}(\rho_{\text{in}}) = \rho_{\text{out}}$, we have $\text{tr}(\rho_{\text{in}}^2) = \text{tr}(\rho_{\text{out}}^2)$. The corresponding, real noisy operation, $\mathcal{G}_{\text{noisy}}$, however, is described by a more general Completely Positive (CP) map, such that for $\mathcal{G}_{\text{noisy}}(\rho_{\text{in}}) = \rho_{\text{out}}$, we have $\text{tr}(\rho_{\text{out}}^2) \leq \text{tr}(\rho_{\text{in}}^2)$. The reduction in purity of states when acted on by a noisy channel is related to the *unitarity* of such channel, a measure of “how far” $\mathcal{G}_{\text{noisy}}$ is from being unitary. Because locally we can always relate a noisy channel with an ideal gate by $\mathcal{G}_{\text{noisy}} := \mathcal{E} \circ \mathcal{G}$ ([1]) for some CP map \mathcal{E} , the unitarity of the noisy gate equivalently measures how far \mathcal{E} is from being unitary.

The average unitarity of a quantum channel can be defined as in [12], by

$$\bar{u}(\mathcal{E}) := \frac{2^n}{2^n - 1} \mathbb{E}_{\psi \sim \text{Haar}} \|\mathcal{E}'(\psi)\|_2^2, \quad (1)$$

where $\mathcal{E}'(\cdot) := \mathcal{E}(\cdot - \mathbb{1}/2^n)$, with $\mathbb{1}$ being an n -qubit identity operator, and the normalization $2^n/(2^n - 1)$ ensuring that $0 \leq \bar{u}(\mathcal{E}) \leq 1$, and with $\bar{u}(\mathcal{E}) = 1$ if and only if \mathcal{E} —and hence the noisy operation $\mathcal{G}_{\text{noisy}}$ —is unitary. Since the purity of a noisy output state may be written in the form $\text{tr}(\rho_{\text{out}}^2) = \|\mathcal{E}(\rho_{\text{in}})\|_2^2$, the definition in Eq. (1) implies that the average purity of a noisy state is, in general, a combination of average unitarity and trace-decrease and/or non-unital terms¹.

¹See, e.g., Eq. (26) for an explicit expression.

The unitarity only quantifies *how unitary* $\mathcal{G}_{\text{noisy}}$ is, but not whether it is the target unitary, i.e., it does not measure whether $\mathcal{G}_{\text{noisy}}$ is far from the ideal \mathcal{G} . A figure of merit aiming to quantify this distinction is the average gate fidelity,

$$\begin{aligned} \bar{F}(\mathcal{G}_{\text{noisy}}, \mathcal{G}) &:= \mathbb{E}_{\psi \sim \text{Haar}} \text{tr}[\mathcal{G}_{\text{noisy}}(\psi)\mathcal{G}(\psi)] \\ &= \mathbb{E}_{\psi \sim \text{Haar}} \langle \psi | \mathcal{E}(\psi) | \psi \rangle := \bar{F}(\mathcal{E}), \end{aligned} \quad (2)$$

where implicitly we denote $\bar{F}(\mathcal{E}) := \bar{F}(\mathcal{E}, \mathcal{I})$, the average gate fidelity of \mathcal{E} with respect to the identity \mathcal{I} (and in a slight abuse of notation, $\psi = |\psi\rangle\langle\psi|$). The average gate fidelity satisfies $1/(2^n + 1) \leq \bar{F}(\mathcal{E}) \leq 1$, with $\bar{F}(\mathcal{E}) = 1$ if and only if $\mathcal{E} = \mathcal{I}$ (equivalently if and only if $\mathcal{G}_{\text{noisy}} = \mathcal{G}$). With respect of \bar{F} , in [12] it is shown that the average unitarity satisfies $\bar{u}(\mathcal{E}) \geq \bar{f}(\mathcal{E})^2$, where

$$\bar{f}(\mathcal{E}) = \frac{2^n \bar{F}(\mathcal{E}) - 1}{2^n - 1}, \quad (3)$$

is the so-called average polarization of \mathcal{E} , and with saturation occurring for a depolarizing (purely incoherent) channel.

The unitarity can also be written in terms of fidelity as $\bar{u}(\mathcal{E}) = (2^n/(2^n - 1))\bar{F}(\mathcal{E}'^\dagger\mathcal{E}')$, where \mathcal{E}'^\dagger is the adjoint map of \mathcal{E}' ². Thus, the average unitarity can also be understood as a type of second-order function of the fidelity of \mathcal{E}' , quantifying on average how distinguishable is the composition $\mathcal{E}'^\dagger\mathcal{E}'$ from the identity. Under the assumptions that \mathcal{E} approximately models the average noise of a gate set $\{\mathcal{G}_i\}$ in a temporally uncorrelated (Markovian), time-independent and gate-independent way, $\bar{F}(\mathcal{E})$ can be estimated through RB, and the unitarity $\bar{u}(\mathcal{E})$ can be estimated through URB [12, 16]. Neither technique is scalable in the number of qubits, however, recently the MRB and BiRB variants were developed in [21–23] allowing efficient and scalable estimation of at least $\bar{F}(\mathcal{E})$ for a large number of qubits.

2 Pauli noise unitarity

Incoherent noise is Trace Preserving (TP) and unital, and a distinction from coherent noise is

²The adjoint map Φ^\dagger of a CP map Φ is defined by $\text{tr}[A\Phi(B)] = \text{tr}[\Phi^\dagger(A)B]$, or equivalently by conjugating the Kraus operators of Φ .

that it generates no net rotation of the state space [1]. Pauli noise is a special case of incoherent noise described by a channel $\rho \mapsto \sum_{P \in \text{Pauli}_n} \alpha_P P \rho P$, where α_P is the Pauli error probability associated to a n -qubit Pauli operator P . Its relevance stems not only from that of the Pauli basis in quantum information theory and experiment but also from its extensive application in quantum error characterization [35–41], quantum error mitigation [3–7], quantum error correction [9, 42, 43] and in its connection with fault tolerance thresholds [11, 13, 14, 44, 45]. Any quantum channel \mathcal{E} can be averaged to a corresponding Pauli channel \mathcal{E}° by means of its Pauli twirl, $\mathcal{E} \mapsto \mathcal{E}^\circ(\cdot) := \sum_{P \in \text{Pauli}_n} 4^{-n} P \mathcal{E}(P \cdot P) P$, i.e., reduced to a Pauli channel with the same Pauli error probabilities as \mathcal{E} .

Result 1 (Fidelity bound for Pauli unitarity). The unitarity of the *Pauli-twirled* channel \mathcal{E}° of \mathcal{E} is bounded by

$$\bar{f}(\mathcal{E})^2 \leq \bar{u}(\mathcal{E}^\circ) \leq \frac{4^n - 2}{(2^n - 1)^2} \bar{r}(\mathcal{E})^2 + \bar{f}(\mathcal{E})^2, \quad (4)$$

where \bar{f} is average polarization defined by Eq. (3), and $\bar{r} := 1 - \bar{F}$ is average infidelity.

The proof is detailed in Appendix G. Given an average layer (in)fidelity, the bound in Ineq. (4) allows us to estimate whether average noise is close to Pauli through the average unitarity. Furthermore, the Pauli-twirled channel \mathcal{E}° of a given *noise* channel \mathcal{E} can be efficiently approximated operationally by Randomized Compiling (RC) [15, 17], so Ineq. (4) enables to certify RC through the average unitarity. Generally, for small average infidelity, Ineq. (4) will be tight, and the average unitarity will need to approach the square of the average polarization, $\bar{f}(\mathcal{E})^2$, for the average noise to be strictly Pauli. This can be seen more clearly for a fixed number of qubits n , as in Fig. 2.

The upper bound in Ineq. (4) overestimates the average unitarity of Pauli noise by a proportion of cross-products of non-identity Pauli error rates, $(\sum \alpha_P)^2 - \sum \alpha_P^2$, and further assumes TP noise, so while a unitarity outside the Pauli bounds guarantees that average noise will contain coherent error contributions, a unitarity value within the Pauli interval (4) solely points to the likelihood of the average noise being Pauli.

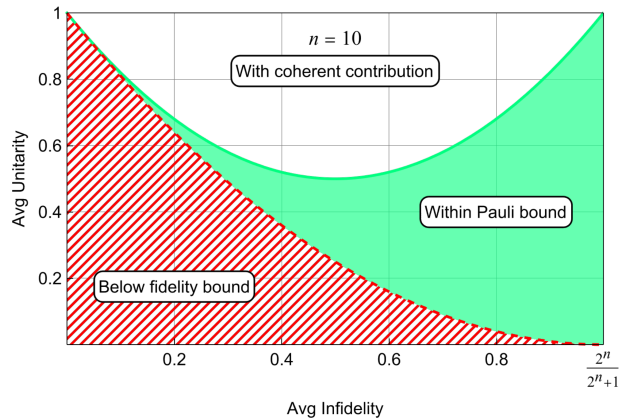


Figure 2: **Pauli unitarity region with respect to infidelity (case $n = 10$ qubits).** Regions for all possible pairs of average unitarity and fidelity: the dashed red region denotes all impossible combinations for Markovian CP noise, the green shaded region denotes values within Ineq. (4) for the average unitarity of Pauli noise, and the white region denotes all values outside such bound, guaranteed to contain coherent error contributions.

3 Purity and fidelity via randomized measurements

The main roadblock for a scalable URB stems from purity being a quadratic function of a quantum state, in general requiring knowledge of all its components, e.g., as described in [12] requiring state tomography within a RB protocol. The efficient estimation of purity, however, was one of the first problems giving rise to the RM and shadow tomography techniques [27, 30, 31]. While for the particular case of purity, the number of required measurements for a given accuracy still scales exponentially, the exponent for RMs is significantly smaller than for full tomography [27].

We will focus on the result of [32, 33],

$$\text{tr}(\rho^2) = 2^n \sum_{\mathbf{s}, \mathbf{s}'} (-2)^{-h(\mathbf{s}, \mathbf{s}')} \mathbb{E}_{\mathbf{U}_i \sim \text{Haar}} \mathbf{P}_{\mathbf{U}}^{(\mathbf{s})} \mathbf{P}_{\mathbf{U}}^{(\mathbf{s}')}, \quad (5)$$

where here $\mathbf{U} = \otimes_{i=1}^n \mathbf{U}_i$ is a random unitary, with $\mathbb{E}_{\mathbf{U}_i \sim \text{Haar}}$ denoting averaging with the Haar measure over the each \mathbf{U}_i , \mathbf{s} and \mathbf{s}' are n -bit strings, $h(\mathbf{s}, \mathbf{s}')$ is the Hamming distance (number of distinct bits) between them, and the

$$\mathbf{P}_{\mathbf{U}}^{(\mathbf{s})} := \langle \mathbf{s} | \mathbf{U}^\dagger \rho \mathbf{U} | \mathbf{s} \rangle, \quad (6)$$

are probabilities of observing the n -bit string \mathbf{s} upon randomizing with \mathbf{U} , and which are estimated in experiment. Since Eq. (5) involves two

copies of U and U^\dagger , it suffices that the local unitaries U_i belong to a unitary 2-design [46], such as the uniformly-distributed Clifford group.

By a RM, here we will mean a random unitary operation U , followed by a projective measurement in the computational basis, $U|s\rangle$ ³. In Eq. (6), this can equivalently be read as randomizing the state ρ with $V = U^\dagger$, and then performing a computational basis measurement.

Purity can alternatively be estimated through the so-called *shadow* of the state, constructed via RMs. That is, one can equivalently construct proxy states $\hat{\rho}_s$ through the probabilities $P_U(s)$ and compute the purity through products $\text{tr}(\hat{\rho}_s \hat{\rho}_{s'})$ [26]. This is an equivalent approach with similar performance guarantees [27]; here we employ Eq. (5) because it can be used within a RB-like protocol straightforwardly.

Operationally, the purity is truly important once in light of an associated fidelity [48]: notice that the probabilities $P_U^{(s)}$ can be *recycled* in a straightforward way to estimate the fidelity of ρ with respect to an ideal pure state $|\psi\rangle$, through a slight modification to Eq. (5), as

$$\langle \psi | \rho | \psi \rangle = 2^n \sum_{s, s'} (-2)^{-h(s, s')} \mathbb{E}_{U_i \sim \text{Haar}} P_U^{(s)} Q_U^{(s')}, \quad (7)$$

where here now $Q_U^{(s)} = |\langle \psi | U | s \rangle|^2$ is the probability of observing the n -bit string s upon randomizing with $U = \otimes_i U_i$ and measuring $|\psi\rangle$. This comes at the expense of estimating the ideal probabilities $Q_U^{(s)}$, but this can be done classically in an efficient way since the U_i can be replaced by single-qubit Clifford unitaries.

4 Average unitarity through randomized measurement correlations

While we do not require the same setup as in MRB or BiRB, we mainly follow the framework and notation of [22]. We will, in particular, only consider single-qubit and two-qubit gate sets, \mathbb{G}_1 and \mathbb{G}_2 , distributed according to probability distributions Ω_1 and Ω_2 , respectively. We will refer to instructions with these gate sets on n -qubits,

³More strictly, this corresponds to a RM *element*, and the concept of a RM can be formalized with Random Positive Operator Valued Measurement (POVM)s, as in [47]

simply as *layers*, and denote the corresponding set of layers by $\mathbb{L}(\mathbb{G})$, where $\mathbb{G} = \mathbb{G}_1 \cup \mathbb{G}_2$. In practice, a rule on how to apply the sampled gates must also be specified, depending e.g., on the topology, connectivity, and the desired density of the gates.

We construct n -qubit random circuits, of layer circuit circuit depth m , of the form

$$C_m = L_m L_{m-1} \cdots L_1, \quad (8)$$

where the right-hand side is read (or acts) from right to left, and where each $L_i = L_i^{(2)} L_i^{(1)}$ is a composite layer, made up of subsequent applications of a layer $L_i^{(1)} \in \mathbb{L}(\mathbb{G}_1)$, of only parallel single-qubit gates, and a layer $L_i^{(2)} \in \mathbb{L}(\mathbb{G}_2)$, of only parallel two-qubit gates. We will say that all $L_i \in \mathbb{L}(\mathbb{G})$ are random layers distributed according to Ω , which is such that $\Omega(L_i) = \Omega_1(L_i^{(1)}) \Omega_2(L_i^{(2)})$, and we refer to C_m in Eq. (8) as a Ω -distributed random circuit of depth m .

We use the term *depth* to mean the number of layers entering the given Ω -distributed circuit, *before* transpilation to a given basis gate set. We illustrate these concepts in Fig. 3. We also point out that while the choice of the pair (\mathbb{G}, Ω) is a priori arbitrary, here we will only consider $\mathbb{G}_1 := \text{Clif}_1$ being the Clifford group (or effectively any other efficient single-qubit unitary 2-design) and Ω_1 a uniform distribution.

Finally, below we distinguish estimators of expectation values of a random variable by a circumflex, i.e., \hat{X} represents the estimator of the expectation of some random variable X .

4.1 The protocol

With this setup, the protocol consists of:

1. *Preparation*: Generate $N_{C_m^*}$ samples of n -qubit Ω -distributed circuits C_m for all given circuit depths m , each with a different layer $V \in \mathbb{L}(\text{Clif}_1)$ sampled uniformly, prepended to it. We will denote $C_m^* := C_m V$.

2. *Quantum Execution*: Estimate probabilities

$$P_{W, C_m^*}^{(s)} := \langle s | W C_m V (|0\rangle\langle 0|) V^\dagger C_m^\dagger W^\dagger | s \rangle, \quad (9)$$

of observing the n -bit string s , for all circuit depths m , all $N_{C_m^*}$ circuit samples and a given

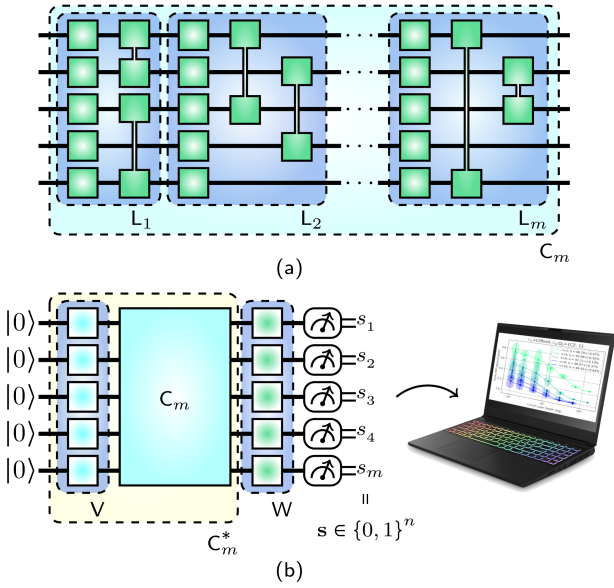


Figure 3: Ω -distributed circuits and RMs: In (a), a sketch of a sample of a ($n = 5$ qubit) Ω -distributed circuit C_m , as a sequence of random layers $L_1, L_2, \dots, L_m \sim \Omega$ made up of only parallel (according to device topology) layers of single- and two-qubit gates, G_1 and G_2 , respectively, sampled according to their corresponding distributions Ω_1 and Ω_2 . In (b), a layer of random single-qubit Clifford gates V is prepended to the circuit C_m , defining a circuit C_m^* , and the final measurement is randomized with a different layer of random single-qubit Clifford gates W , generating a n -bit string s ; a set of such measurements can be processed according to Protocol 4.1 to estimate the average unitarity of the corresponding Ω -distributed circuits.

number N_W of layer samples $W \in \mathbb{L}(G_1)$, sampled according to Ω_1 . We denote the corresponding estimator quantities, given a finite number of measurements N_{meas} by

$$\hat{P}_{W, C_m^*}^{(s)} = \frac{1}{N_{\text{meas}}} \sum_{i=1}^{N_{\text{meas}}} \mathbf{1}_s(\mathbf{x}_i), \quad (10)$$

where \mathbf{x}_i is a random variable describing the i^{th} projective measurement of the n -qubits in the computational basis, with $\mathbf{1}_s(\mathbf{x}) = 1$ if $\mathbf{x} = \mathbf{s}$ or 0 otherwise.

3. *Classical post-processing*: Estimate the average purity $\text{tr}(\rho_m^2)$ for all depth m states $\rho_m := C_m V(|0\rangle\langle 0|) V^\dagger C_m^\dagger$, via

$$\hat{\mathfrak{P}}_m = 2^n \sum_{\substack{\mathbf{s}, \mathbf{s}' \\ W, C_m^*}} \frac{(-2)^{-h(\mathbf{s}, \mathbf{s}')} \hat{P}_{W, C_m^*}^{(\mathbf{s})} \hat{P}_{W, C_m^*}^{(\mathbf{s}')}}{N_W N_{C_m^*}}, \quad (11)$$

where $h(\mathbf{s}, \mathbf{s}')$ is the number of distinct elements between the n -bit strings \mathbf{s} and \mathbf{s}' . Estimate the probabilities $\hat{Q}_{W, C_m^*}^{(\mathbf{s})} := |\langle \mathbf{s} | W^{(\text{id})} | \psi_m^{(\text{id})} \rangle|^2$ for all noiseless states, $\psi_m^{(\text{id})} := C_m^{(\text{id})} V^{(\text{id})} |0\rangle$ of depth m —with the label (id) here denoting noiseless quantities—, and the corresponding average fidelities $\langle \psi_m | \rho_m | \psi_m \rangle$, via

$$\hat{\mathfrak{F}}_m = 2^n \sum_{\substack{\mathbf{s}, \mathbf{s}' \\ W, C_m^*}} \frac{(-2)^{-h(\mathbf{s}, \mathbf{s}')} \hat{P}_{W, C_m^*}^{(\mathbf{s})} \hat{Q}_{W, C_m^*}^{(\mathbf{s}')}}{N_W N_{C_m^*}}. \quad (12)$$

Both estimators can be rendered unbiased and improved by other considerations as in § 4.3.

Whenever the Ω -distributed circuits are generated by layers containing non-Clifford gates in a way that becomes impractical to simulate (e.g., whereby there is a high density of such non-Cliffords or for a large number of qubits), the average layer fidelity can alternatively be estimated through MRB [22]; the trade-off is having to construct and measure corresponding mirror circuits. The estimations of Protocol 4.1 and MRB by definition will agree upon employing the same ensemble of layers; in Appendix F we numerically observe such agreement.

Result 2 (Exponential decay). Throughout Appendices B, C and D we show that, under the circumstances detailed below,

$$\mathbb{E}_\Omega \text{tr}(\rho_m^2) \approx A \bar{u}(\mathcal{E})^m + \frac{1}{2^n}, \quad (13)$$

where $0 \leq A \leq 1$, and

$$\bar{u}(\mathcal{E}) = \frac{2^n \bar{F}(\mathcal{E}^\dagger \mathcal{E}) - 1}{2^n - 1} = \bar{f}(\mathcal{E}^\dagger \mathcal{E}) \quad (14)$$

is the average layer unitarity of the noise, where $\mathcal{E} := \mathcal{L}_{i_{\text{noisy}}} \mathcal{L}_i^\dagger$ is approximately the noise channel corresponding to any layer L_i with associated map $\mathcal{L}_i(\cdot) := L_i(\cdot) L_i^\dagger$, and $\bar{F}(\mathcal{E}^\dagger \mathcal{E})$ is the average fidelity of $\mathcal{E}^\dagger \mathcal{E}$ with respect to the identity.

Similarly, the decay in average fidelity can be seen to correspond to

$$\mathbb{E}_\Omega \langle \psi_m | \rho_m | \psi_m \rangle \approx \alpha \bar{f}(\mathcal{E})^m + \frac{1}{2^n}, \quad (15)$$

where $0 \leq \alpha \leq 1$, similar to a usual RB decay for unital SPAM.

In such case, the estimators in Eq. (11) and Eq. (12) of protocol 4.1, can be fit to the respective decays in depth m , whereby both average layer unitarity and fidelity can be estimated.

4.1.1 Conditions for an exponential decay

While a general functional form in terms of *any* Markovian noise model for the average sequence purity and fidelity can be obtained, as in Appendices B, C and D, ensuring that it will follow a simple exponential decay as in Eq. (13) relies on the noise satisfying certain approximate conditions and the pair (\mathbb{G}, Ω) having certain properties, similar to any RB-based technique. Aside from standard assumptions such as Markovianity (i.e., that noise is not temporally correlated), time-independence and weak gate-dependence⁴, Result 2 requires the following:

- A₁. That noise is approximately trace-preserving and unital, i.e., without significant leakage or entropy-decreasing contributions.
- A₂. That the Ω -distributed circuits approximate a unitary 2-design, to the effect that $\mathbb{E}_{L \sim \Omega} \mathcal{L}^\dagger \mathcal{X} \mathcal{L}(\cdot) \approx p(\cdot) + (1-p)\mathbb{1}/2^n$, where $p \leq 1$ only dependent on \mathcal{X} ; i.e., the average composition of noisy layers is approximately equivalent to a depolarizing channel encoding some information about \mathcal{X} . This is formalized and discussed in Appendix E.

Assumption A₁. implies that the purity decay only depends on the unitarity of the average noise, and not on its non-unital or trace-decreasing contribution. Otherwise, if this condition is not satisfied, the average unitarity will not be described by Eq. (14), but rather the most general Eq. (1), and the purity decay will be a convex combination of average unitarity and trace-decreasing contributions of the average noise, as expressed by Eq. (41) of Appendix B (in agreement with [12]). The implications for the fidelity estimation in this case are similar, since the polarization factor would not be described by Eq. (3) but rather a more general $\bar{f}_t(\mathcal{E}) = (2^n \bar{F}(\mathcal{E}) - t)/(2^n - 1)$ for $t = \text{tr}[\mathcal{E}(\mathbb{1}/2^n)]$ quantifying how non-TP the channel is [50]. In other words, the main implication is that the fitting procedure would generally be slightly more

⁴Here meaning with time- and gate-dependent contributions being negligible on average; see e.g., [49].

complicated for non-unital, non-TP noise.

Assumption A₂. implies that we can identify $\bar{u}(\mathcal{E}) = p^2$ as given by Eq. (14), i.e., the average unitarity is simply equal to the polarization of the average composition of noisy layers. This assumption is slightly stronger than that in [21–23, 51], and generally means that up to the second moment and a small positive ϵ , the Ω -distributed circuits we employ should reproduce the statistics of the uniform Haar measure on the unitary group on the n qubits. While the choice of (\mathbb{G}_1, Ω_1) being the uniform single-qubit Clifford group already generates separately a unitary 2-design on each qubit (projecting noise to a Pauli channel [52]), the choice (\mathbb{G}_2, Ω_2) should be such that the random Ω -distributed circuits are *highly scrambling*, as defined in [22, 23], which can be achieved by it containing at least an entangling gate with high probability. While this does not ensure that the circuits will approximate a unitary 2-design in an increasing number of qubits, it suffices in practice for *mid-scale systems*. This is discussed in detail in Appendix E.

4.2 Mid-scale

In § 6, we will discuss the reasons why Protocol 4.1 is practical and feasible for *at least* 10-qubits and generally within tenths of qubits, which is what we refer to as *mid-scale*. This is in the sense that all classical aspects, i.e., steps 1 and 3 can be managed with a standard current-technology laptop and with the quantum execution requiring a mild number of circuits, RMs, and measurement shot samples, as exemplified in § 5.

4.3 Unbiased and Median of Means estimators

There are at least two simple but effective ways in which reliable results can be ensured through the estimators in Eq. (11) and Eq. (12): *i*) using unbiased estimators⁵ and *ii*) using Median of Means (MoMs) estimators.

In [53] it is pointed out that, even though

⁵An estimator of some statistical parameter is said to be *unbiased* or *faithful* when its expectation matches the real expected value of the parameter, or otherwise it is said to be biased.

the probability estimator in Eq. (10) is faithful, i.e. $\mathbb{E}[\hat{P}] = P$ (where we have dropped all indices), it is biased for any other positive integer power. A unique unbiased estimator can nevertheless be built for any power, and in particular, $\hat{P}_2 := \hat{P}(\hat{P}N_{\text{meas}} - 1) / (N_{\text{meas}} - 1)$ is an unbiased estimator of P^2 . Thus all terms in Eq. (11) and Eq. (12) for the n -bit string $\mathbf{s} = \mathbf{s}'$ should be computed through \hat{P}_2 to render average sequence fidelity and purity estimations unbiased.

On the other hand, a simple but highly effective way to reduce the uncertainty associated to a mean estimator is to use MoMs estimators: given K samples of estimators $\hat{\mathfrak{F}}_m^{(1)}, \dots, \hat{\mathfrak{F}}_m^{(K)}$ for the average fidelity of circuits of depth m in Eq. (12), the MoMs estimator of such samples is $\hat{\mathfrak{F}}_m^{\text{MoMs}(K)} := \text{median}(\hat{\mathfrak{F}}_m^{(1)}, \dots, \hat{\mathfrak{F}}_m^{(K)})$, or similarly for the case of the average purity in Eq. (11). In total, this requires $N_W N_{C_m^*} K$ circuit samples to be measured N_{meas} times, which however, is generally more robust compared with simply constructing an empirical estimator of the mean with the same amount of samples [26]. While it has been noted that when measurements are randomized with the single-qubit Clifford group both types of estimators converge similarly to the true mean [54], MoMs has the concentration property of the probability of observing outliers from the true mean decreasing exponentially in K [55].

5 Experiment on IQM Spark™

We now demonstrate the execution of Protocol 4.1 through both an experiment on IQM Spark™ [34], a commercial 5-qubit superconducting quantum system by IQM targeting education in quantum computing; technical details of the hardware can be seen in [56]. The five qubits in the IQM Spark™ are connected in a star-shape, with a central qubit connected to the four remaining qubits. The experiments were performed at specific dates, pointed out where the respective results are displayed, and only reflect the performance of the hardware at such point in time.

We generated Ω -distributed circuits using the gate set $\mathbb{G} = \text{Clif}_1 \cup \{\text{CZ}\}$, with Clif_1 being the uniformly-distributed single-qubit Clifford group (i.e., Ω_1 assigning 1/24 probability for each Clif-

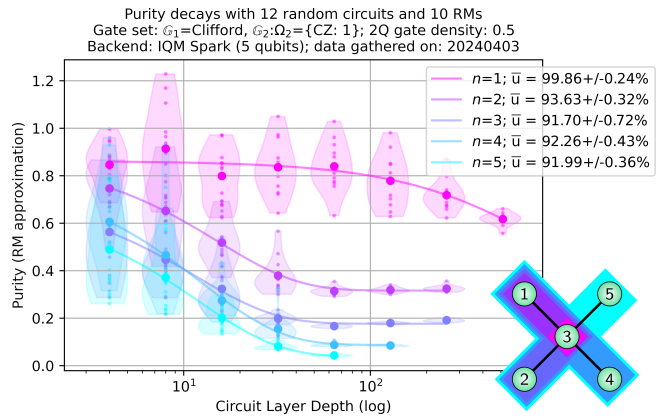


Figure 4: **Purity decays on IQM Spark™**. Computed according to Protocol 4.1 for Ω -distributed circuits with gate set $\mathbb{G} = \text{Clif}_1 \cup \{\text{CZ}\}$, with Clif_1 being the uniformly-distributed single-qubit Clifford group. Individual plots correspond to a given number of qubits taken from a connectivity graph shown in the inset, whereby smaller points correspond to MoMs estimators of purity in Eq. (11) at a given depth m , bigger points correspond to the average purity, violins show the distribution of the MoMs estimators, and lines correspond to a least-squares fit of the averages to the model in Eq. (13), with which the corresponding average unitarities \bar{u} are estimated. Sample parameters: $N_{C_m^*} = 12$, $N_W = 10$, $N_{\text{meas}} = 2^{11}$ and $K = 1, 2$ (for $n = 1, 2, 3$ and $n = 4, 5$ respectively) MoMs.

ford and Ω_2 probability 1 of sampling CZ). The sampling of layers was done employing the edge-graph sampler, defined in [57], with a two-qubit gate density (the expected proportion of qubits occupied by two-qubit gates) of 1/2. The edge-graph sampler considers layers with two-qubit gates only on connected qubits, and where a single logical layer consists of a parallel mixture of one- and two-qubit gates (sampled according to Ω), i.e., there is no more than one gate acting on a given qubit in any layer.

The native set of gates is $\{r_{\theta, \varphi}, \text{CZ}\}$, where $r_{\theta, \varphi}$ is a single-qubit rotation of angle θ around the $\cos(\varphi)X + \sin(\varphi)Y$ axis, CZ is a controlled-Z two-qubit gate. The measurement operator is a computational basis projective measurement operation, and a barrier object is used to prevent the layers defined through \mathbb{G} from being compiled together. The definition of *depth* that we adopt is that of the number of layers defined through \mathbb{G} , i.e., before transpilation to the native gate set.

We extracted decay rates of the average state fidelity and purity in increasing layer depths according to Protocol 4.1, and thus layer fidelity

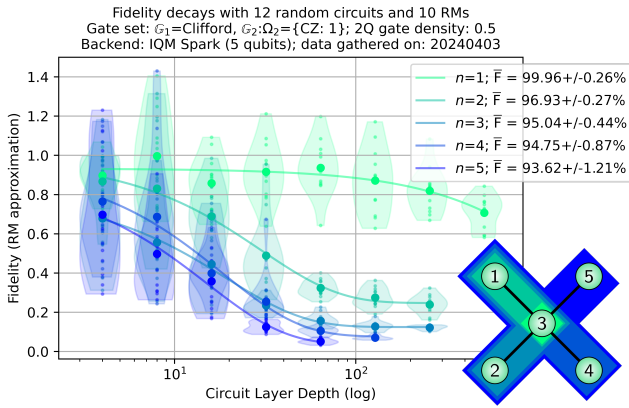


Figure 5: **Fidelity decays on IQM Spark™**. Fidelity decays according to Protocol 4.1 corresponding to the same Ω -distributed circuits and parameters giving probabilities with purities displayed in Fig. 8; here similarly individual plots correspond to a given number of qubits n , small points correspond to Median of Means (MoMs) estimators of (12) at the given depth, larger points correspond to the respective average purity, and lines correspond to least-squares fit of the averages to the model in Eq. (15), whereby the corresponding average layer fidelity \bar{F} in the respective number of qubits n is extracted according to Eq. (3).

and unitarity, for Ω -distributed circuits in arbitrary combinations of $n = 1, 2, \dots, 5$ qubits. In both cases, the sample parameters we employ are $N_{C_m^*} = 12$ random Ω -distributed circuits, times $N_W = 10$ randomized measurement layers, and times $N_{\text{meas}} = 2^{11}$ shots per measurement; we furthermore employ unbiased estimators for square probabilities and either $K = 1$ for $n = 1, 2, 3$ or $K = 2$ for $n = 4, 5$ Median of Means (MoMs) estimators.

In Fig. 4 we show the purity decays in increasing circuit depth for each number of qubits, determined via the estimators in Eq. (11), where, by fitting the decay model in Eq. (13) to the averages, we estimate the corresponding average unitarity. It is worth noticing that we used no median of means for up to three qubits, and thus the individual smaller points in the plot do not represent purities as these have not been averaged over all circuit samples; this is a reason why the violin distributions can stretch beyond 1. Nevertheless, it is expected for the spread in individual outputs to be larger for larger values of purity. Importantly, while averages (larger points) do not all fall exactly on the respective exponential (particularly for $n = 1$), deviations do not appear alarmingly high. Finally, SPAM contributions can be

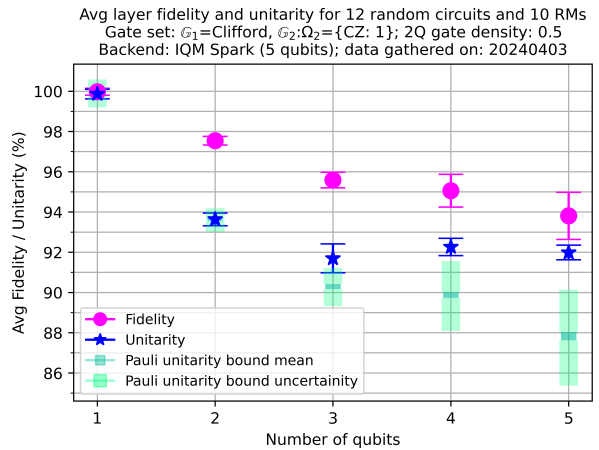


Figure 6: **Average layer fidelities and average unitarities on IQM Spark™**. All estimated average layer fidelities and unitarities, extracted experimentally through Protocol 4.1, in increasing number of qubits are shown, together with ranges of values for potential Pauli unitarities, computed with the estimated fidelities according to Ineq. (4).

seen to lead to a shift in the offset of the curve for $n = 3$.

It is important to notice that in Fig. 4, the unitarity does not appear to be monotonically decreasing in qubit count. In this case, however, this apparent increase could also be explained away by the uncertainty of the data and could be at most a plateau in unitarity; a way to decrease the uncertainties could be by increasing the number of MoMs. This is nevertheless an interesting feature and one that could be investigated further also in the context of determining crosstalk or other types of correlations at the unitarity level.

Following this, in Fig. 5 we show the respective fidelity decays, computed together with the measurement counts from the same experiment and the estimation of the corresponding noiseless probabilities, according to estimator in Eq. (12). Similarly here, the distributions tend to show a larger spread for smaller n , where only the averages represent the corresponding fidelity estimation. While the decays display different SPAM contributions, the averages do decrease in system size; the uncertainties could similarly be reduced e.g., by increasing the amount of MoMs. In Appendix F.3.1 we compare with MRB results gathered weeks before, showing qualitative agreement despite a clear difference in the respective distributions. Since error bars remain relatively

large for fidelities, and hence for the estimated Pauli unitarity intervals, an alternative could be to construct mirror circuits (without the RM Clifford gates appended) within the same experiment and then instead estimate fidelities via MRB for smaller uncertainties.

This finally enables us to get an overall picture of both average layer fidelities and unitarities, together with an estimation of whether noise falls within the Pauli unitarity bound in Eq. (4) or it contains a larger coherent contribution. In Fig. 6 we plot together the average outputs retrieved in Fig. 4 and Fig. 5, together with estimations of Pauli unitarity bounds given the average fidelity estimates, computed via Eq. (4). Fig. 6 gives an overall picture of a coherent noise budget, which could in turn inform the overhead of Pauli twirling techniques. It is relevant to notice that both it is possible for the average unitarity to increase even without there being necessarily correlations between qubits, and that generally the coherence of noise could remain relatively large with respect to fidelity for larger systems.

6 Scaling bottlenecks

6.1 Sample Complexity

The main roadblock for estimating the average coherence of noise in large systems (or even just the purity of quantum states) with RMs, is the required number of measurements to have an estimation within a given error, i.e., its sample complexity, which is then by definition manifested by the variance associated to such RMs. In Protocol 4.1, statistical uncertainty stems from the sampling of the Ω -distributed circuits, that of the RM elements, and the number of measurements per RM element; these quantities correspond to $N_{C_m^*}$ and N_W in the estimators of Eq. (12) and Eq. (11), and to N_{meas} of Eq. (10), respectively.

The main limitation to scalability is imposed by N_{meas} : using local RMs via Eq. (5) to estimate purity to precision $1/\sqrt{N_W}$, it was observed numerically in [33] that it scales approximately as $N_{\text{meas}} \sim 2^{0.75n}$ in number of qubits n . Generally, within the classical shadows framework, the required number of measurements can be seen to scale exponentially in a similar fraction of n and linearly in the actual purity of the

state [26, 58, 59].

Mixedness reduces the sample complexity, as also observed numerically in [33], and with Ω -distributed circuits, quantum states will naturally get increasingly mixed in increasing depth. Coincidentally, thus, a high percentage of coherent error contributes to a higher variance not only in average fidelity estimation but also in average unitarity estimation itself.

When it comes to Ω -distributed circuit samples when estimating average fidelity, the variance associated with it can be directly linked to the average amount of coherent noise [12, 22]. How to control this uncertainty, as well as guarantees when choosing the number of sample circuits and number of measurements, has been widely studied for Clifford RB [10, 49, 60]; furthermore, [16] obtained a bound on the variance for the purity in circuits within (an improved version of) Clifford URB, assuming unital noise. While we are not aware of analogous bounds on the variance for scalable RB (namely employing Ω -distributed circuits), it has been observed numerically that similar behavior follows (at least when layers are made up only of either generators-of or Clifford gates themselves) [22, 23], and that *Pauli twirling* [15, 61] generally suppresses the variance of expectation values under any sequence of operations, regardless of whether noise is correlated (either spatially or temporally) or not [62].

A prospect could therefore be to benchmark average Pauli-dressed gates, aiming to obtain a unitarity within Ineq. (4), with the trade-off being to sample an extra number of Pauli layers per circuit. Here we do not attempt to derive a *rigorous* bound on the variance for the average layer unitarity, but as we have demonstrated experimentally in § 5, while for a given total number of samples the uncertainty is larger for the unitarity than for fidelity, estimating it nevertheless remains tractable for *mid-scale* systems.

6.2 Practical bottlenecks

There are two other *practical* considerations to take into account to estimate at which scale Protocol 3 remains feasible: the SPAM factors in the exponential decay in Eqs. (13),(15), and the number of terms entering in the sum of Eqs. (11),(12).

While our technique gives SPAM-independent estimates of the average unitarity, it can nevertheless make the exponential decays drop way too quickly, so that fitting becomes unfeasible. This is a shared problem of all RB-based techniques, and other than simply improving readouts and/or state preparation, there could be ways of removing the 2^{-n} offset, for example, but the multiplicative factor is still determined by the unitarity of the SPAM⁶. More than a RB problem this might be an issue in general when trying to estimate global, high-weight properties on large systems, essentially because signal readouts eventually become too small.

On the other hand, while Eq. (5) and Eq. (6) are remarkable mathematically, in practice they involve a sum over all possible pairs of n -bit strings. Naively, this means summing up 4^n probability terms; for the case of the purity, this can be reduced at least to $2^{n-1}(2^n - 1)$, given that the Hamming distance is symmetric. This computation can be done easily on a classical machine in parallel, but it can also become rather unpractical (as it furthermore would need to be done for every single purity estimate). While this is a practical problem, it is fundamentally tied to the fact that the purity of a state involves all the elements of the density matrix.

7 Conclusions

We have derived an upper bound on the average unitarity of Pauli-twirled noise solely in terms of the average fidelity of the respective bare noise, and we have established a protocol enabling the estimation of the average unitarity for a broad class of quantum circuits in digital systems, independent of technology platform or architecture, with tenths of qubits. Our results have been inspired both by novel scalable Randomized Benchmarking (RB) techniques, as well as Randomized Measurements (RM) methods. We have shown that reliable estimation of both average operation coherence and fidelity in such systems can be done under mild conditions and with a reasonable

⁶For example, if we assume that SPAM noise (i.e. that which we would attribute to the initial and final single-qubit-only layers) is global depolarizing (as done for MRB [22]) with polarization p , then the multiplicative factor in Eq. (13) is $A \lesssim p^4$.

sampling overhead. Finally, we demonstrated our results in experiment on up to 5 qubits and numerically in simulation with up to 10 qubits.

A fully scalable estimation of the average coherence of noise will almost surely rely on modularity, e.g., by using smaller-scale unitarity information extracted from smaller qubit subsets and then combined with a Simultaneous RB-like protocol.

A promising way of moving forward in this direction is that of [59], where the authors establish a method to estimate entropy and entanglement of a quantum state in polynomially-many measurements, relying on conditions essentially satisfied when spatial correlation lengths in the system remain finite and for systems in a one-dimensional topology. Their main result suggests that generally one could partition *any* large n -qubit system into smaller subsystems and reconstruct the global n -qubit purity from the *local* purity of pairs of contiguous subsystems, like *stitching* together the bigger purity with a number of measurements that overall grow polynomially in n . As a direct consequence, if such results hold more generally, our protocol could be used to estimate global average noise coherence with a similar sample complexity.

Nevertheless, several things remain unclear, e.g., what classes of (Markovian) noise such a method would hold for, how it could be phrased beyond one-dimensional qubit arrays, or how one would certify the global purity estimations, among others. As we have argued, however, the average coherence of noise is a crucial figure of merit for benchmarking the error mechanisms limiting the performance of quantum computers, perhaps only standing after average layer fidelity in terms of importance as a benchmark, so the aforementioned hurdles must soon be overcome.

Acknowledgments

The authors acknowledge support from the German Federal Ministry of Education and Research (BMBF) under Q-Exa (grant No. 13N16062) and QSolid (grant No. 13N16161). The authors also acknowledge the entire IQM Technology team for their support in the development of this work.

References

- [1] R. Blume-Kohout, M. P. da Silva, E. Nielsen, T. Proctor, K. Rudinger, M. Sarovar, and K. Young. “A taxonomy of small Markovian errors”. *PRX Quantum* **3**, 020335 (2022).
- [2] K. Rudinger, C. W. Hogle, R. K. Naik, A. Hashim, D. Lobser, D. I. Santiago, M. D. Grace, E. Nielsen, T. Proctor, S. Seritan, S. M. Clark, R. Blume-Kohout, I. Siddiqi, and K. C. Young. “Experimental characterization of crosstalk errors with simultaneous gate set tomography”. *PRX Quantum* **2**, 040338 (2021).
- [3] K. Temme, S. Bravyi, and J. M. Gambetta. “Error mitigation for short-depth quantum circuits”. *Phys. Rev. Lett.* **119**, 180509 (2017).
- [4] B. McDonough, A. Mari, N. Shammah, N. T. Stemen, M. Wahl, W. J. Zeng, and P. P. Orth. “Automated quantum error mitigation based on probabilistic error reduction”. In 2022 IEEE/ACM Third International Workshop on Quantum Computing Software (QCS). IEEE (2022).
- [5] A. Gonzales, R. Shaydulin, Z. H. Saleem, and M. Suchara. “Quantum error mitigation by Pauli check sandwiching”. *Sci. Rep.* **13** (2023).
- [6] E. van den Berg, S. Bravyi, J. M. Gambetta, P. Jurcevic, D. Maslov, and K. Temme. “Single-shot error mitigation by coherent Pauli checks”. *Phys. Rev. Res.* **5**, 033193 (2023).
- [7] E. van den Berg, Z. K. Mineev, A. Kandala, and K. Temme. “Probabilistic error cancellation with sparse Pauli–Lindblad models on noisy quantum processors”. *Nat. Phys.* (2023).
- [8] E. Knill. “Quantum computing with realistically noisy devices”. *Nature* **434**, 39–44 (2005).
- [9] B. Eastin. “Error channels and the threshold for fault-tolerant quantum computation” (2007). [arXiv:0710.2560](https://arxiv.org/abs/0710.2560).
- [10] J. J. Wallman and S. T. Flammia. “Randomized benchmarking with confidence”. *New J. Phys.* **16**, 103032 (2014).
- [11] Y. R. Sanders, J. J. Wallman, and B. C. Sanders. “Bounding quantum gate error rate based on reported average fidelity”. *New J. Phys.* **18**, 012002 (2015).
- [12] J. J. Wallman, C. Granade, R. Harper, and S. T. Flammia. “Estimating the coherence of noise”. *New J. Phys* **17**, 113020 (2015).
- [13] R. Kueng, D. M. Long, A. C. Doherty, and S. T. Flammia. “Comparing experiments to the fault-tolerance threshold”. *Phys. Rev. Lett.* **117**, 170502 (2016).
- [14] A. Hashim, S. Seritan, T. Proctor, K. Rudinger, N. Goss, R. K. Naik, J. M. Kreikebaum, D. I. Santiago, and I. Siddiqi. “Benchmarking quantum logic operations relative to thresholds for fault tolerance”. *npj Quantum Inf.* **9** (2023).
- [15] J. J. Wallman and J. Emerson. “Noise tailoring for scalable quantum computation via randomized compiling”. *Phys. Rev. A* **94**, 052325 (2016).
- [16] B. Dirkse, J. Helsen, and S. Wehner. “Efficient unitarity randomized benchmarking of few-qubit Clifford gates”. *Phys. Rev. A* **99**, 012315 (2019).
- [17] A. Hashim, R. K. Naik, A. Morvan, J.-L. Ville, B. Mitchell, J. M. Kreikebaum, M. Davis, E. Smith, C. Iancu, K. P. O’Brien, I. Hincks, J. J. Wallman, J. Emerson, and I. Siddiqi. “Randomized compiling for scalable quantum computing on a noisy superconducting quantum processor”. *Phys. Rev. X* **11**, 041039 (2021).
- [18] J. Eisert, D. Hangleiter, N. Walk, I. Roth, D. Markham, R. Parekh, U. Chabaud, and E. Kashefi. “Quantum certification and benchmarking”. *Nat. Rev. Phys.* **2**, 382–390 (2020).
- [19] M. Kliesch and I. Roth. “Theory of quantum system certification”. *PRX Quantum* **2**, 010201 (2021).
- [20] J. Helsen, I. Roth, E. Onorati, A.H. Werner, and J. Eisert. “General framework for randomized benchmarking”. *PRX Quantum* **3**, 020357 (2022).
- [21] T. Proctor, S. Seritan, K. Rudinger, E. Nielsen, R. Blume-Kohout, and K. Young. “Scalable randomized benchmarking of quantum computers using mirror circuits”. *Phys. Rev. Lett.* **129**, 150502 (2022).
- [22] J. Hines, M. Lu, R. K. Naik, A. Hashim, J.-L. Ville, B. Mitchell, J. M. Krikebaum, D. I. Santiago, S. Seritan, E. Nielsen, R. Blume-Kohout, K. Young, I. Siddiqi, B. Whaley, and T. Proctor. “Demonstrating scalable

- randomized benchmarking of universal gate sets”. *Phys. Rev. X* **13**, 041030 (2023).
- [23] J. Hines, D. Hothem, R. Blume-Kohout, B. Whaley, and T. Proctor. “Fully scalable randomized benchmarking without motion reversal” (2023). [arXiv:2309.05147](https://arxiv.org/abs/2309.05147).
- [24] D. C. McKay, I. Hincks, E. J. Pritchett, M. Carroll, L. C. G. Govia, and S. T. Merkel. “Benchmarking quantum processor performance at scale” (2023). [arXiv:2311.05933](https://arxiv.org/abs/2311.05933).
- [25] J. Hines and T. Proctor. “Scalable full-stack benchmarks for quantum computers” (2023). [arXiv:2312.14107](https://arxiv.org/abs/2312.14107).
- [26] H.-Y. Huang, R. Kueng, and J. Preskill. “Predicting many properties of a quantum system from very few measurements”. *Nat. Phys.* **16**, 1050–1057 (2020).
- [27] A. Elben, S. T. Flammia, H.-Y. Huang, R. Kueng, J. Preskill, B. Vermersch, and P. Zoller. “The randomized measurement toolbox”. *Nat. Rev. Phys.* **5**, 9–24 (2022).
- [28] J. Helsen, M. Ioannou, J. Kitzinger, E. Onorati, A. H. Werner, J. Eisert, and I. Roth. “Shadow estimation of gate-set properties from random sequences”. *Nat. Commun.* **14**, 5039 (2023).
- [29] G. A. L. White, K. Modi, and C. D. Hill. “Filtering crosstalk from bath non-Markovianity via spacetime classical shadows”. *Phys. Rev. Lett.* **130**, 160401 (2023).
- [30] S. J. van Enk and C. W. J. Beenakker. “Measuring $\text{Tr}\rho^n$ on single copies of ρ using random measurements”. *Phys. Rev. Lett.* **108**, 110503 (2012).
- [31] A. Elben, B. Vermersch, M. Dalmonte, J. I. Cirac, and P. Zoller. “Rényi entropies from random quenches in atomic hubbard and spin models”. *Phys. Rev. Lett.* **120**, 050406 (2018).
- [32] T. Brydges, A. Elben, P. Jurcevic, B. Vermersch, C. Maier, B. P. Lanyon, P. Zoller, R. Blatt, and C. F. Roos. “Probing Rényi entanglement entropy via randomized measurements”. *Science* **364**, 260–263 (2019).
- [33] A. Elben, B. Vermersch, C. F. Roos, and P. Zoller. “Statistical correlations between locally randomized measurements: A toolbox for probing entanglement in many-body quantum states”. *Phys. Rev. A* **99**, 052323 (2019).
- [34] “IQM quantum computers: IQM spark™”. <https://www.meetiqm.com/products/iqm-spark>. Accessed: 2024-04-17.
- [35] S. T. Flammia and Y.-K. Liu. “Direct fidelity estimation from few Pauli measurements”. *Phys. Rev. Lett.* **106**, 230501 (2011).
- [36] A. Chiuri, V. Rosati, G. Vallone, S. Pádua, H. Imai, S. Giacomini, C. Macchiavello, and P. Mataloni. “Experimental realization of optimal noise estimation for a general Pauli channel”. *Phys. Rev. Lett.* **107**, 253602 (2011).
- [37] S. T. Flammia and J. J. Wallman. “Efficient estimation of Pauli channels”. *ACM Transactions on Quantum Computing* **1**, 1–32 (2020).
- [38] R. Harper, S. T. Flammia, and J. J. Wallman. “Efficient learning of quantum noise”. *Nat. Phys.* **16**, 1184–1188 (2020).
- [39] R. Harper, W. Yu, and S. T. Flammia. “Fast estimation of sparse quantum noise”. *PRX Quantum* **2**, 010322 (2021).
- [40] S. Chen, Y. Liu, M. Otten, A. Seif, B. Fefferman, and L. Jiang. “The learnability of Pauli noise”. *Nat. Commun.* **14** (2023).
- [41] E. van den Berg and P. Wocjan. “Techniques for learning sparse Pauli-lindblad noise models” (2023). [arXiv:2311.15408](https://arxiv.org/abs/2311.15408).
- [42] S. J. Beale, J. J. Wallman, M. Gutiérrez, K. R. Brown, and R. Laflamme. “Quantum error correction decoheres noise”. *Phys. Rev. Lett.* **121**, 190501 (2018).
- [43] T. Wagner, H. Kampermann, D. Bruß, and M. Kliesch. “Pauli channels can be estimated from syndrome measurements in quantum error correction”. *Quantum* **6**, 809 (2022).
- [44] M. Gutiérrez and K. R. Brown. “Comparison of a quantum error-correction threshold for exact and approximate errors”. *Phys. Rev. A* **91**, 022335 (2015).
- [45] D. K. Tuckett, S. D. Bartlett, and S. T. Flammia. “Ultrahigh error threshold for surface codes with biased noise”. *Phys. Rev. Lett.* **120**, 050505 (2018).
- [46] C. Dankert, R. Cleve, J. Emerson, and E. Livine. “Exact and approximate unitary 2-designs and their application to fidelity estimation”. *Phys. Rev. A* **80**, 012304 (2009).
- [47] T. Heinosaari, M. A. Jivulescu, and I. Nechita. “Random positive operator valued measures”. *J. Math. Phys.* **61** (2020).
- [48] C. Di Franco and M. Paternostro. “A no-go

- result on the purification of quantum states”. *Sci. Rep.* **3** (2013).
- [49] E. Magesan, J. M. Gambetta, and J. Emerson. “Characterizing quantum gates via randomized benchmarking”. *Phys. Rev. A* **85**, 042311 (2012).
- [50] Joel J. Wallman. “Randomized benchmarking with gate-dependent noise”. *Quantum* **2**, 47 (2018).
- [51] A. M. Polloreno, A. Carignan-Dugas, J. Hines, R. Blume-Kohout, K. Young, and T. Proctor. “A theory of direct randomized benchmarking” (2023). [arXiv:2302.13853](https://arxiv.org/abs/2302.13853).
- [52] J. M. Gambetta, A. D. Córcoles, S. T. Merkel, B. R. Johnson, John A. Smolin, J. M. Chow, C. A. Ryan, C. Rigetti, S. Poletto, T. A. Ohki, M. B. Ketchen, and M. Steffen. “Characterization of addressability by simultaneous randomized benchmarking”. *Phys. Rev. Lett.* **109**, 240504 (2012).
- [53] B. Vermersch, A. Elben, M. Dalmonte, J. I. Cirac, and P. Zoller. “Unitary n -designs via random quenches in atomic Hubbard and spin models: Application to the measurement of Rényi entropies”. *Phys. Rev. A* **97**, 023604 (2018).
- [54] A. Zhao, N. C. Rubin, and A. Miyake. “Fermionic partial tomography via classical shadows”. *Phys. Rev. Lett.* **127**, 110504 (2021).
- [55] M. Lerasle. “Lecture notes: Selected topics on robust statistical learning theory” (2019). [arXiv:1908.10761](https://arxiv.org/abs/1908.10761).
- [56] Jami Rönkkö, Olli Ahonen, Ville Bergholm, Alessio Calzona, Attila Geresdi, Hermanni Heimonen, Johannes Heinsoo, Vladimir Milchakov, Stefan Pogorzalek, Matthew Sarsby, Mykhailo Savytskyi, Stefan Seegerer, Fedor Šimkovic IV, P. V. Sriluckshmy, Panu T. Vesanen, and Mikio Nakahara. “On-premises superconducting quantum computer for education and research” (2024). [arXiv:2402.07315](https://arxiv.org/abs/2402.07315).
- [57] T. Proctor, K. Rudinger, K. Young, E. Nielsen, and R. Blume-Kohout. “Measuring the capabilities of quantum computers”. *Nat. Phys.* **18**, 75–79 (2021).
- [58] A. Elben, R. Kueng, H.-Y. Huang, R. van Bijnen, C. Kokail, M. Dalmonte, P. Calabrese, B. Kraus, J. Preskill, P. Zoller, and B. Vermersch. “Mixed-state entanglement from local randomized measurements”. *Phys. Rev. Lett.* **125**, 200501 (2020).
- [59] B. Vermersch, M. Ljubotina, J. I. Cirac, P. Zoller, M. Serbyn, and L. Piroli. “Many-body entropies and entanglement from polynomially-many local measurements”. *Phys. Rev. X* **14**, 031035 (2024).
- [60] J. Helsen, J. J. Wallman, S. T. Flammia, and S. Wehner. “Multiqubit randomized benchmarking using few samples”. *Phys. Rev. A* **100**, 032304 (2019).
- [61] M. Ware, G. Ribeill, D. Ristè, C. A. Ryan, B. Johnson, and M. P. da Silva. “Experimental Pauli-frame randomization on a superconducting qubit”. *Phys. Rev. A* **103**, 042604 (2021).
- [62] P. Figueroa-Romero, M. Papič, A. Auer, M.-H. Hsieh, K. Modi, and I. de Vega. “Operational Markovianization in Randomized Benchmarking” *Quantum Sci. Technol.* **9**, 035020 (2024).
- [63] F. G. S. L. Brandão, A. W. Harrow, and M. Horodecki. “Local random quantum circuits are approximate polynomial-designs”. *Commun. Math. Phys.* **346**, 397–434 (2016).
- [64] J. Haferkamp. “Random quantum circuits are approximate unitary t -designs in depth $O(nt^{5+o(1)})$ ”. *Quantum* **6**, 795 (2022).
- [65] J. Emerson, R. Alicki, and K. Życzkowski. “Scalable noise estimation with random unitary operators”. *Journal of Optics B: Quantum and Semiclassical Optics* **7**, S347 (2005).
- [66] M. A Nielsen. “A simple formula for the average gate fidelity of a quantum dynamical operation”. *Physics Letters A* **303**, 249–252 (2002).
- [67] T. Proctor, S. Seritan, E. Nielsen, K. Rudinger, K. Young, R. Blume-Kohout, and M. Sarovar. “Establishing trust in quantum computations” (2022). [arXiv:2204.07568](https://arxiv.org/abs/2204.07568).
- [68] P. Figueroa-Romero, K. Modi, and M.-H. Hsieh. “Towards a general framework of Randomized Benchmarking incorporating non-Markovian Noise”. *Quantum* **6**, 868 (2022).
- [69] S. T. Flammia. “Averaged circuit eigenvalue sampling” (2021). [arXiv:2108.05803](https://arxiv.org/abs/2108.05803).

A Preliminaries

Here we detail and expand on some of the notation and technical details that go into showing the results claimed in the main text. Much of the structure for the circuits entering the protocol is inspired by [21, 22], so for this reason we stick to most of the original terminology and notation.

A.1 Ω -distributed circuits

We will consider a quantum system made up of $n \geq 2$ qubits and a pair of single-qubit and two-qubit gate sets, \mathbb{G}_1 and \mathbb{G}_2 , respectively, with corresponding probability distributions Ω_1 and Ω_2 . We will then generate quantum circuits by sampling from $\mathbf{g}_1 \sim \Omega_1$ and $\mathbf{g}_2 \sim \Omega_2$, to generate parallel instructions on the n qubits as specified by a set $\mathbb{L}(\mathbb{G}) = \{L_i = L_i^{(1)}L_i^{(2)}\}$, where each $L_i^{(1)} \in \mathbb{L}(\mathbb{G}_1)$ and $L_i^{(2)} \in \mathbb{L}(\mathbb{G}_2)$ are instructions made up of only the single and two-qubit gates \mathbf{g}_1 and \mathbf{g}_2 , respectively. To stress when some quantities are random variables, we use sans font when relevant, as in L_i being a random layer sampled from Ω , which is such that $\Omega(L_i) = \Omega_1(L_i^{(1)})\Omega_2(L_i^{(2)})$.

Circuits generated this way, here for the particular case $\mathbb{G} = (\mathbb{G}_1, \mathbb{G}_2)$ and $\Omega = (\Omega_1, \Omega_2)$, are said to be Ω -distributed circuits, e.g., the circuit as stated in the main text as

$$C_m = L_m L_{m-1} \cdots L_1, \quad (16)$$

where each $L_i \in \mathbb{L}(\Omega)$ sampled according to Ω , and the right-hand-side is read from right to left (i.e., C_m is an operator acting onto quantum states on the left), is a Ω -distributed circuit of depth m .

We point out that, in general, Ω -distributed circuits can be constructed with an arbitrary number of gate sets and their corresponding distributions. Moreover, while so far $\mathbb{G}_1, \mathbb{G}_2$ and Ω_1, Ω_2 are completely up to the user to specify, in practice the main requirements we will have on this choice are that, *i*) the resulting Ω -distributed circuits constitute an ϵ -approximate unitary 2-design, and *ii*) that in particular (\mathbb{G}_1, Ω_1) is an exact unitary 2-design, e.g., the single-qubit Clifford group. As such conditions *i*) and *ii*) are considered *a posteriori* for a particular case of interest, we will have a general derivation and then these will be stated formally in point 3 of § B.4 and in § C.2, respectively.

A.2 Ideal vs real implementations

While we do not stress this difference in the main text, here we will denote by U_L an ideal (noiseless) unitary operator associated to a representation of the layer L , and by $\mathcal{U}_L(\rho) := U_L \rho U_L^\dagger$ the action of its corresponding map or superoperator \mathcal{U}_L .

We write a composition of two maps \mathcal{A} and \mathcal{B} simply as $\mathcal{B}\mathcal{A}$ to mean “apply map \mathcal{B} after applying map \mathcal{A} ”, equivalent to the usual notations $\mathcal{B} \circ \mathcal{A}$, or $\mathcal{B}(\mathcal{A}(x))$.

Noisy implementations of layers will generally be denoted by a map ϕ , e.g., the noisy application of a layer L is denoted by the Completely Positive (CP) map (which we also refer to as a quantum channel, or simply, a channel) $\phi(L)$, which can be defined (see e.g., §IV of [1]) such that $\phi(L) := \mathcal{E}_L \mathcal{U}_L$, with \mathcal{E}_L being generally a CP map associated to L .

A.3 The output states of Ω -distributed circuits

We will consider a set of Ω -distributed circuits of depth m , acting on a fiducial initial state $|0\rangle$, which in turn we randomize with a layer $V \in \mathbb{L}(\mathbb{G}_1)$. That is, we will have circuits of the form $C_m V |0\rangle$, which will always give a pure state output in the noiseless case. In the noisy case, however, we will have

states of the form

$$\tilde{\varrho}_m := \mathbb{E}_{\substack{\mathbf{L}_i \sim \Omega \\ \mathbf{V} \sim \Omega_1}} \phi(\mathbf{L}_m) \phi(\mathbf{L}_{m-1}) \cdots \phi(\mathbf{L}_1) \phi(\mathbf{V}) (|0\rangle\langle 0|), \quad (17)$$

averaged independently over each of the Ω -distributed layers \mathbf{L}_i , and uniformly over the initial single-qubit gate layer $\mathbf{V} \in \mathbb{L}(\mathbb{G}_1)$ with Ω_1 . This noisy output can of course now be mixed, $2^{-N} \leq \text{tr}(\tilde{\varrho}_m^2) \leq 1$.

Our protocol focuses on efficiently estimating the purities of the states $\tilde{\varrho}_m$, to in turn estimate the average unitarity of noise in the circuits \mathbf{C}_m . In the following, we first study the behavior of the average purity of $\tilde{\varrho}_m$ in increasing circuit depth m , and then we see that we can efficiently estimate this quantity employing Randomized Measurements (RM)s, allowing us to readily extract the average unitarity of noise in certain circumstances which we analyze.

B Purity of average outputs of Ω -distributed circuits

B.1 Purity of the initial randomization

Let us consider first the case of no gate layers but just the noisy initial single-qubit Clifford layer, $m = 0$, then we have

$$\begin{aligned} \text{tr}(\tilde{\varrho}_0^2) &= \mathbb{E}_{\mathbf{V} \sim \Omega_1} \text{tr}[\phi(\mathbf{V})(|0\rangle\langle 0|)\phi(\mathbf{V})(|0\rangle\langle 0|)^\dagger] \\ &:= \mathbb{E}_{\psi \sim \Omega_1} \text{tr}[\mathcal{E}_{\text{spam}}(|\psi\rangle\langle\psi|)\mathcal{E}_{\text{spam}}(|\psi\rangle\langle\psi|)^\dagger], \end{aligned} \quad (18)$$

where we defined the noisy implementation of \mathbf{V} as $\phi(\mathbf{V}) := \mathcal{E}_{\text{spam}} \mathcal{U}_{\mathbf{V}}$ for some noise channel $\mathcal{E}_{\text{spam}}$ explicitly standing for State Preparation and Measurement (SPAM) noise, and where we defined the initial randomized pure state as $\mathcal{U}_{\mathbf{V}}(|0\rangle\langle 0|) := |\psi\rangle\langle\psi|$.

Noticing that the noisy outputs $\mathcal{E}_{\text{spam}}(|\psi\rangle\langle\psi|)$ are quantum states and thus Hermitian, and that we can define the self-adjoint map \mathcal{X}^\dagger of a quantum channel \mathcal{X} by the property $\text{tr}[A\mathcal{X}(B)] := \text{tr}[\mathcal{X}^\dagger(A)B]$, we can write

$$\text{tr}(\tilde{\varrho}_0^2) = \mathbb{E}_{\psi \sim \Omega_1} \langle \psi | \mathcal{E}_{\text{spam}}^\dagger \mathcal{E}_{\text{spam}} (|\psi\rangle\langle\psi|) | \psi \rangle. \quad (19)$$

Equivalently, the self-adjoint map of a quantum channel can be defined in terms of its Kraus operators as $\mathcal{X}^\dagger(\cdot) := \sum K_\mu^\dagger(\cdot)K_\mu$, where $\{K_\mu\}$ the Kraus operators of \mathcal{X} , so Eq. (19) in a sense is already measuring how different $\mathcal{E}_{\text{spam}}$ is from a unitary.

In general, the purity of a quantum state, $\rho := \mathcal{X}(|\varphi\rangle\langle\varphi|)$ can be written as $\text{tr}(\rho^2) := \langle \varphi | \mathcal{X}^\dagger \mathcal{X} (|\varphi\rangle\langle\varphi|) | \varphi \rangle$, which corresponds to the gate fidelity of $\mathcal{X}^\dagger \mathcal{X}$ with respect to the identity on the state $|\varphi\rangle$. Thus, we can write Eq. (19) as a gate-fidelity of $\mathcal{E}_{\text{spam}}^\dagger \mathcal{E}_{\text{spam}}$ with respect to the identity, averaged over all possible initial states $|\psi\rangle$,

$$\text{tr}(\tilde{\varrho}_0^2) = \mathbb{E}_{\psi \sim \Omega_1} F_\psi(\mathcal{E}_{\text{spam}}^\dagger \mathcal{E}_{\text{spam}}), \quad (20)$$

where here

$$F_\psi(\mathcal{X}) := \langle \psi | \mathcal{X} (|\psi\rangle\langle\psi|) | \psi \rangle, \quad (21)$$

is the gate-fidelity of the map \mathcal{X} with respect to the identity map on the state $|\psi\rangle$.

B.2 Relation to average unitarity and average trace-decrease

Ultimately, however, the average loss of purity in the average state $\tilde{\varrho}_0$ must be related to some amount of *non-unitarity* of the noise, i.e., it is noise that decreases purity. This can be quantified by the average

unitarity, $\mathbb{E}_{|\psi\rangle} \mathbf{u}_\psi$, defined for a CP map \mathcal{E} as

$$\mathbb{E}_{\psi \sim \Omega_1} \mathbf{u}_\psi(\mathcal{E}) := \left(\frac{2^n}{2^n - 1} \right) \mathbb{E}_{\psi \sim \Omega_1} F_\psi(\mathcal{E}'^\dagger \mathcal{E}'), \quad \text{where } \mathcal{E}'(\cdot) := \mathcal{E}(\cdot - \mathbb{1}/2^n), \quad (22)$$

which is so defined to account for the case of \mathcal{E} being trace-decreasing. When \mathcal{E} is Trace Preserving (TP) we have the relation $\mathcal{E}'^\dagger \mathcal{E}'(\cdot) = \mathcal{E}^\dagger \mathcal{E}(\cdot - \mathbb{1}/2^n)$, otherwise, however, for any quantum state ρ ,

$$\mathcal{E}'^\dagger \mathcal{E}'(\rho) = \mathcal{E}^\dagger \mathcal{E} \left(\rho - \frac{\mathbb{1}}{2^n} \right) - \text{tr} \left[\mathcal{E} \left(\rho - \frac{\mathbb{1}}{2^n} \right) \right] \mathcal{E}^\dagger \left(\frac{\mathbb{1}}{2^n} \right), \quad (23)$$

thus

$$\begin{aligned} \left(\frac{2^n - 1}{2^n} \right) \mathbb{E}_{\psi \sim \Omega_1} \mathbf{u}_\psi(\mathcal{E}) &= \mathbb{E}_{\psi \sim \Omega_1} F_\psi(\mathcal{E}^\dagger \mathcal{E}) \\ &\quad - \mathbb{E}_{\psi \sim \Omega_1} \langle \psi | \mathcal{E}^\dagger \mathcal{E}(\mathbb{1}/2^n) | \psi \rangle - \mathbb{E}_{\psi \sim \Omega_1} \text{tr} [\mathcal{E}'(|\psi\rangle\langle\psi|)] \langle \psi | \mathcal{E}^\dagger(\mathbb{1}/2^n) | \psi \rangle \\ &= \mathbb{E}_{\psi \sim \Omega_1} F_\psi(\mathcal{E}^\dagger \mathcal{E}) - 2^{-n} \mathbb{E}_{\psi \sim \Omega_1} \left\{ \mathcal{S}_\psi(\mathcal{E}^\dagger \mathcal{E}) + \mathcal{S}_\psi(\mathcal{E}) [\mathcal{S}_\psi(\mathcal{E}) - \text{tr}[\mathcal{E}(\mathbb{1}/2^n)]] \right\}, \end{aligned} \quad (24)$$

where

$$\mathcal{S}_\psi(\mathcal{E}) := \text{tr}[\mathcal{E}(|\psi\rangle\langle\psi|)], \quad (25)$$

is a trace-preservation measure of the map \mathcal{E} for a given sample $|\psi\rangle$.

We can then write the average purity of $\tilde{\rho}_0$ as

$$\begin{aligned} \text{tr}(\tilde{\rho}_0^2) &= \left(\frac{2^n - 1}{2^n} \right) \mathbb{E}_{\psi \sim \Omega_1} \mathbf{u}_\psi(\mathcal{E}_{\text{spam}}) \\ &\quad + 2^{-n} \mathbb{E}_{\psi \sim \Omega_1} \left\{ \mathcal{S}_\psi(\mathcal{E}_{\text{spam}}^\dagger \mathcal{E}_{\text{spam}}) + \mathcal{S}_\psi(\mathcal{E}_{\text{spam}}) [\mathcal{S}_\psi(\mathcal{E}_{\text{spam}}) - \text{tr}[\mathcal{E}_{\text{spam}}(\mathbb{1}/2^n)]] \right\}, \end{aligned} \quad (26)$$

which we recall is defined as averaged over the states $|\psi\rangle\langle\psi| = \mathcal{U}_V(|0\rangle\langle 0|)$, which are distributed uniformly and independently on the n -qubits according to a distribution Ω_1 on single-qubit gates \mathbb{G}_1 .

When the noise channel \mathcal{E} is TP, the rightmost summand in Eq. (24) becomes a term equal to -2^{-n} , and in that case the average unitarity is just a re-scaling of the average gate-fidelity of the form

$$\mathbb{E}_{\psi \sim \Omega_1} \mathbf{u}_\psi(\mathcal{E}) \stackrel{(\mathcal{E} \text{ is TP})}{=} \frac{2^n \mathbb{E}_{\psi \sim \Omega_1} F_\psi(\mathcal{E}^\dagger \mathcal{E}) - 1}{2^n - 1}. \quad (27)$$

and thus also the average purity in Eq. (20) in this case would become

$$\text{tr}(\tilde{\rho}_0^2) \stackrel{(\mathcal{E}_{\text{spam}} \text{ is TP})}{=} \left(\frac{2^n - 1}{2^n} \right) \mathbb{E}_{\psi \sim \Omega_1} \mathbf{u}_\psi(\mathcal{E}_{\text{spam}}) + \frac{1}{2^n}. \quad (28)$$

B.3 The case of global depolarizing noise

A particular case of a quantum channel for modeling noise that is both easy mathematically as in interpretation is that of global depolarizing channel,

$$\mathcal{E}_p(\cdot) := p(\cdot) + (1 - p) \text{tr}(\cdot) \frac{\mathbb{1}}{2^n}, \quad (29)$$

where $0 \leq p \leq 1$ is the probability for the input state to remain the same, and which can be directly defined in terms of the channel by the so-called polarization γ ,

$$\gamma(\mathcal{E}) := \frac{4^n F_{\text{ent}}(\mathcal{E}) - 1}{4^n - 1}, \quad (30)$$

where here

$$\mathbf{F}_{\text{ent}}(\mathcal{E}) := \langle \Psi | (\mathcal{I} \otimes \mathcal{E}) [|\Psi\rangle\langle\Psi|] | \Psi \rangle, \quad \text{where } |\Psi\rangle := \frac{\sum_{i=1}^{2^n} |ii\rangle}{\sqrt{2^n}}, \quad (31)$$

is the so-called entanglement fidelity (equivalent to the purity of the so-called Choi state of \mathcal{E}). Because maximally entangled states can be written in the Pauli basis as $|\Psi\rangle\langle\Psi| = 4^{-n} \sum_{P \in \text{Pauli}_n} P \otimes P^T$, this is equivalent to

$$\mathbf{F}_{\text{ent}}(\mathcal{E}) = \frac{1}{4^n} \sum_{P \in \text{Pauli}_n} \frac{1}{2^n} \text{tr}[P\mathcal{E}(P)] = \frac{1}{4^n} \text{tr}(\mathcal{E}), \quad (32)$$

where we identified the matrix \mathcal{E} , with elements $\mathcal{E}_{ij} = \frac{1}{2^n} \text{tr}[P_i\mathcal{E}(P_j)]$, as the Pauli Transfer Matrix representation of \mathcal{E} .

For a depolarizing channel, in particular,

$$\gamma(\mathcal{E}_p) = p. \quad (33)$$

Also, a composition of depolarizing channels with the same polarization is just another depolarizing channel as

$$\underbrace{\mathcal{E}_p \cdots \mathcal{E}_p}_{k \text{ times}} = \mathcal{E}_{p^k}. \quad (34)$$

Given the above property, for a depolarizing channel, we also have

$$\begin{aligned} \mathbf{u}_\psi(\mathcal{E}_p) &= \frac{2^n \mathbf{F}_\psi(\mathcal{E}_{p^2}) - 1}{2^n - 1} \\ &= \gamma(\mathcal{E}_p)^2 \\ &:= \mathbf{u}(\mathcal{E}_p), \end{aligned} \quad (35)$$

for any state $|\psi\rangle$. To stress this independence of the state ψ , we drop the subindex in the last line, which simply means $\mathbf{u}(\mathcal{E}_p) := \mathbf{u}_\varphi(\mathcal{E}_p)$ for an arbitrary pure state $|\varphi\rangle$.

Notice that, $\mathcal{E}_p \mathcal{U}_C = \mathcal{U}_C \mathcal{E}_p$, or more generally,

$$\mathcal{E}_p \mathcal{X} = \mathcal{X} \mathcal{E}_p, \quad (36)$$

whenever \mathcal{X} is a unital and TP quantum channel. Furthermore, for any unital and TP channel \mathcal{X} , the unitarity $\mathbf{u}_\psi(\mathcal{E}_p \mathcal{X})$ only depends on $\mathbf{F}_\psi(\mathcal{X}^\dagger \mathcal{E}_{p^2} \mathcal{X})$, which satisfies

$$\begin{aligned} \mathbf{F}_\psi(\mathcal{X}^\dagger \mathcal{E}_{p^2} \mathcal{X}) &= \langle \psi | \mathcal{X}^\dagger \mathcal{E}_{p^2} \mathcal{X} (|\psi\rangle\langle\psi|) | \psi \rangle \\ &= p^2 \mathbf{F}_\psi(\mathcal{X}^\dagger \mathcal{X}) + (1 - p^2) 2^{-n}, \\ &= \mathbf{u}(\mathcal{E}_p) \left(\mathbf{F}_\psi(\mathcal{X}^\dagger \mathcal{X}) - 2^{-n} \right) + 2^{-n}, \end{aligned} \quad (37)$$

and so

$$\mathbf{u}_\psi(\mathcal{E}_p \mathcal{X}) = \frac{2^n \mathbf{u}(\mathcal{E}_p) \left(\mathbf{F}_\psi(\mathcal{X}^\dagger \mathcal{X}) - 2^{-n} \right)}{2^n - 1} = \mathbf{u}(\mathcal{E}_p) \mathbf{u}_\psi(\mathcal{X}), \quad (38)$$

i.e. the unitarity this way for depolarizing channels factorizes.

B.4 Average purity in the many-layer case

We now first consider adding a single layer of gates according to the distribution Ω , and evaluate the purity of $\tilde{\varrho}_1$,

$$\begin{aligned}
\text{tr}(\tilde{\varrho}_1^2) &= \mathbb{E}_{\substack{\mathbf{L}_1 \sim \Omega \\ \mathbf{V} \sim \Omega_1}} \text{tr}[\phi(\mathbf{L}_1)\phi(\mathbf{V})(|0\rangle\langle 0|)\phi(\mathbf{L}_1)\phi(\mathbf{V})(|0\rangle\langle 0|)^\dagger] \\
&= \mathbb{E}_{\substack{\mathbf{L}_1 \sim \Omega \\ \psi \sim \Omega_1}} \text{tr}[\mathcal{E}_1 \mathcal{U}_1 \mathcal{E}_{\text{spam}}(|\psi\rangle\langle\psi|) \mathcal{E}_1 \mathcal{U}_1 \mathcal{E}_{\text{spam}}(|\psi\rangle\langle\psi|)] \\
&= \mathbb{E}_{\substack{\mathbf{L}_1 \sim \Omega \\ \psi \sim \Omega_1}} F_\psi(\mathcal{E}_{\text{spam}}^\dagger \mathcal{U}_1^\dagger \mathcal{E}_1^\dagger \mathcal{E}_1 \mathcal{U}_1 \mathcal{E}_{\text{spam}}). \tag{39}
\end{aligned}$$

This can then be generalized directly to the case of m layers as

$$\text{tr}(\tilde{\varrho}_m^2) = \mathbb{E}_{\substack{\mathbf{L}_1 \sim \Omega \\ \psi \sim \Omega_1}} F_\psi(\mathcal{E}_{\text{spam}}^\dagger \mathcal{U}_1^\dagger \mathcal{E}_1^\dagger \cdots \mathcal{U}_m^\dagger \mathcal{E}_m^\dagger \mathcal{E}_m \mathcal{U}_m \cdots \mathcal{E}_1 \mathcal{U}_1 \mathcal{E}_{\text{spam}}), \tag{40}$$

and thus by means of Eq. (24), this is equivalent to

$$\text{tr}(\tilde{\varrho}_m^2) = \left(\frac{2^n - 1}{2^n}\right) \mathbb{E}_{\substack{\mathbf{L}_i \sim \Omega \\ \psi \sim \Omega_1}} \mathbf{u}_\psi(\mathcal{E}_m \mathcal{U}_m \cdots \mathcal{E}_1 \mathcal{U}_1 \mathcal{E}_{\text{spam}}) + \text{trace decreasing terms}, \tag{41}$$

where the trace decreasing terms are terms in \mathbf{S} that can be read directly from Eq. (24). One can express this way the most general form of the purity of the average state $\tilde{\varrho}_m$ in circuit depth m .

However, we care, of course, for the situation in which the decay is exponential in m with the unitarity as the rate of decay.

1. We may consider first that the noise is approximately gate and time independent, $\mathcal{E}_i \approx \mathcal{E}$, in which case at most we can get a double exponential in $\mathbf{u}(\mathcal{E})$ and $\mathcal{S}(\mathcal{E})$, as in [12]. This approximation can be formalized by assuming that the average over time steps and gates is the leading contribution to the actual noise; see e.g., [49].
2. If we consider noise that is only gate-independent but that is unital and TP, we have

$$\begin{aligned}
\text{tr}(\tilde{\varrho}_m^2) &= \mathbb{E}_{\substack{\mathbf{L}_1 \sim \Omega \\ \psi \sim \Omega_1}} F_\psi(\mathcal{E}_{\text{spam}}^\dagger \mathcal{U}_1^\dagger \mathcal{E}_1^\dagger \cdots \mathcal{U}_m^\dagger \mathcal{E}_m^\dagger \mathcal{E}_m \mathcal{U}_m \cdots \mathcal{E}_1 \mathcal{U}_1 \mathcal{E}_{\text{spam}}) \\
&= \mathbb{E}_{\psi \sim \Omega_1} \langle \psi | \mathbb{E}_{\mathbf{L}_i \sim \Omega} \mathcal{E}_{\text{spam}}^\dagger \mathcal{U}_1^\dagger \mathcal{E}_1^\dagger \cdots \mathcal{U}_m^\dagger \mathcal{E}_m^\dagger \mathcal{E}_m \mathcal{U}_m \cdots \mathcal{E}_1 \mathcal{U}_1 \mathcal{E}_{\text{spam}}(|\psi\rangle\langle\psi|) | \psi \rangle, \tag{42}
\end{aligned}$$

and we can average recursively over each layer.

3. This circuit averaging, however, becomes significant if the layer set at least forms an ϵ -approximate unitary 2-design⁷, to the effect that $\mathbb{E}_{\mathbf{L} \sim \Omega} \mathcal{U}_\mathbf{L}^\dagger \mathcal{E}^\dagger \mathcal{E} \mathcal{U}_\mathbf{L} \approx \tilde{\Xi}_p$ for a global depolarizing channel $\tilde{\Xi}_{p^2}$

⁷A unitary t -design is a probability measure μ on the d -dimensional unitary group $\mathbf{U}(d)$ (or a subset thereof), such that $\mathcal{T}_\mu^{(t)} = \mathcal{T}_{\text{Haar}}^{(t)}$, where $\mathcal{T}_\mu^{(t)}(\cdot) := \int_{\mathbf{U}(d)} d\mu(U) U^{\otimes t}(\cdot)(U^{\otimes t})^\dagger$ is a t -twirl over the unitary group. There are several nonequivalent, albeit often related, ways of approximating unitary designs, here we employ that in [63, 64], where $(1-\epsilon)\mathcal{T}_\mu^{(t)} \preceq \mathcal{T}_{\text{Haar}}^{(t)} \preceq (1+\epsilon)\mathcal{T}_\mu^{(t)}$ with $A \preceq B$ here if and only if $A - B$ is CP, which can be interpreted in a straightforward way as having a small multiplicative factor of difference when measuring a state acted on with $\mathcal{T}_\mu^{(t)}$ vs with $\mathcal{T}_{\text{Haar}}^{(t)}$. Finally, for the case $t = 2$, the 2-twirl on a CP map Φ can be stated in terms of its matrix representation Φ through $\mathcal{T}_\mu^{(2)}(\Phi)$, equivalent to the expression $\int_{\mathbf{U}(d)} d\mu(U) U^\dagger \Phi(U \rho U^\dagger) U$ for any state ρ .

with polarization

$$\begin{aligned}
p^2 &= \frac{\sum |\text{tr}[K_\alpha^\dagger K_\beta]|^2 - 1}{4^n - 1} \\
&= \frac{\text{tr}[\mathcal{E}^\dagger \mathcal{E}] - 1}{4^n - 1} \\
&= \frac{4^n \text{F}_{\text{ent}}(\mathcal{E}^\dagger \mathcal{E}) - 1}{4^n - 1} \\
&= \frac{2^n \bar{\text{F}}(\mathcal{E}^\dagger \mathcal{E}) - 1}{2^n - 1},
\end{aligned} \tag{43}$$

where in the first line $\{K_\mu\}$ are the Kraus operators of \mathcal{E} [65], or equivalently in the second line with \mathcal{E} being a matrix representation of \mathcal{E} ⁸, or in terms of the entanglement fidelity through Eq. (32) in the third line, or finally through the average gate-fidelity [66], as we write in the main text. Thus, if we further consider Ω -distributed circuits that form an approximate unitary 2-design, we may write

$$\text{tr}(\tilde{\rho}_m^2) \approx \mathbb{E}_{\psi \sim \Omega_1} \langle \psi | \mathcal{E}_{\text{spam}}^\dagger \tilde{\Xi}_{p_m^2} \cdots \tilde{\Xi}_{p_1^2} \mathcal{E}_{\text{spam}} (|\psi\rangle\langle\psi|) | \psi \rangle, \tag{44}$$

where the approximation “ \approx ” here neglects the small ϵ multiplicative corrections; due to the property in Eq. (36), and where we intentionally defined the polarizations to be squares, given that $p^2 = u(\tilde{\Xi}_{p_i})$ ⁹. For approximately time-stationary noise, to the effect that all polarizations are equal, $p_1 = \cdots = p_m = p$, this is equivalent to the exponential decay

$$\text{tr}(\tilde{\rho}_m^2) \approx A u(\tilde{\Xi}_p)^m + \frac{1}{2^n}, \tag{45}$$

where $A = 2^{-n}(2^n - 1) \mathbb{E}_{\psi \sim \Omega_1} u_\psi(\mathcal{E}_{\text{spam}})$ is a SPAM constant. Of course, given that $u(\tilde{\Xi}_p) = p^2$, this unitarity can also be expressed by $u(\mathcal{E})$, as done in Eq. (13) in the main text.

C Operational estimation of the purity

Now we know how the purity of the noisy average state $\tilde{\rho}_m$ in Eq. (17) behaves in terms of the average unitarity of noise with respect to circuit depth m . The task is then to estimate this quantity via RMs.

C.1 Purity estimation through randomized measurements

RMs found some of their first applications in estimating the purity of the quantum state of a subsystem [30, 31]. Specifically, here we will focus on the results of [32, 33], whereby it is shown that for a reduced quantum state $\rho_A = \text{tr}_B(\rho_{AB})$, from some composite closed quantum system AB , where here we assume A to be a n -qubit quantum system, its purity can be expressed as

$$\text{tr}(\rho_A^2) = 2^n \sum_{\mathbf{s}, \mathbf{s}'} (-2)^{-h(\mathbf{s}, \mathbf{s}')} \mathbb{E}_{\mathbf{U} \sim \text{Haar}} [\text{P}_{\mathbf{U}}(\mathbf{s}) \text{P}_{\mathbf{U}}(\mathbf{s}')], \tag{46}$$

where \mathbf{s} and \mathbf{s}' are n -bit strings, $h(\mathbf{s}, \mathbf{s}')$ is the Hamming distance (number of distinct bits) between them, $\mathbb{E}_{\mathbf{U} \sim \text{Haar}}$ denotes uniform averaging with the Haar measure over the local unitaries $\mathbf{U} = \otimes_{i=1}^n U_i$,¹⁰ and the

$$\text{P}_{\mathbf{U}}(\mathbf{s}) := \langle \mathbf{s} | \mathcal{U}_{\mathbf{U}}(\rho_A) | \mathbf{s} \rangle, \tag{47}$$

⁸It is possible to identify $\mathcal{X} = \begin{pmatrix} S(\mathcal{E}) & \mathcal{X}_{\text{sdl}} \\ \mathcal{X}_n & \mathcal{X}_{\text{unital}} \end{pmatrix}$, where $S(\mathcal{E})$, \mathcal{X}_{sdl} , \mathcal{X}_n and $\mathcal{X}_{\text{unital}}$ are trace-decreasing, state-dependent leakage, non-unital and unital components (of dimensions 1, $1 \times (4^n - 1)$, $(4^n - 1) \times 1$ and square $(4^n - 1)$), respectively. This leads to the expression in [12] for the average unitarity.

⁹We notice that this does not mean that $\tilde{\Xi}_p$ corresponds to (approximately) the average of a single \mathcal{E} (which only occurs if \mathcal{E} itself is already depolarizing).

¹⁰That is, \mathbb{E}_{Haar} here refers to a uniform and independent average over all the local unitaries U_i with the Haar measure, i.e., $\mathbb{E}_{\text{Haar}} \sim \mathbb{E}_{U_1} \mathbb{E}_{U_2} \cdots \mathbb{E}_{U_N}$

are noiseless probabilities of observing the n -bit string \mathbf{s} upon applying the unitary U on the reduced state ρ_A .

The main advantage here is that the quantum component of estimating purity this way is just the probabilities in Eq. (47), which simply means applying a product of random unitaries and measuring each on a user-specified basis. The rest, i.e., fully estimating Eq. (46) is purely classical post-processing of said probabilities. For n qubits, the number of distinct terms in the sum over n -bit strings in Eq. (46) is $2^{n-1}(2^n - 1)$, since the Hamming distance is symmetric, $h(\mathbf{s}, \mathbf{s}') = h(\mathbf{s}', \mathbf{s})$; however, this sum is only a function of the probabilities P_U , so it could, for example, be computed in parallel.

C.2 Purity of many layer Ω -distributed circuits through randomized measurements

Let us again begin by considering the case $m = 1$, of a single random layer, so that the equivalent of the probability in Eq. (47), by measuring the state $\tilde{\rho}_1$ with a RM using a random unitary $W \in \mathbb{L}(\mathbb{G}_1)$ over Ω_1 , reads as

$$\begin{aligned}
P_{1,W}(\mathbf{s}) &= \text{tr}[\phi(W)(|\mathbf{s}\rangle\langle\mathbf{s}|) \tilde{\rho}_1] \\
&= \mathbb{E}_{\substack{L_1 \sim \Omega \\ V \sim \Omega_1}} \text{tr}[\phi(W)(|\mathbf{s}\rangle\langle\mathbf{s}|) \phi(L_1)\phi(V)(|0\rangle\langle 0|)] \\
&= \mathbb{E}_{\substack{L_1 \sim \Omega \\ \psi \sim \Omega_1}} \text{tr}[\mathcal{E}'_{\text{spam}_w} \mathcal{U}'_W(|\mathbf{s}\rangle\langle\mathbf{s}|) \mathcal{E}_1 \mathcal{U}_1 \mathcal{E}_{\text{spam}_v}(|\psi\rangle\langle\psi|)] \\
&= \mathbb{E}_{\substack{L_1 \sim \Omega \\ \psi \sim \Omega_1}} \langle \mathbf{s} | \mathcal{U}_W \mathcal{E}_{\text{spam}_w} \mathcal{E}_1 \mathcal{U}_1 \mathcal{E}_{\text{spam}_v}(|\psi\rangle\langle\psi|) | \mathbf{s} \rangle, \tag{48}
\end{aligned}$$

where we again defined $\mathcal{U}_V(|0\rangle\langle 0|) = |\psi\rangle\langle\psi|$ as a random (according to a uniform $\mathcal{U}_V \sim \Omega_1$) pure state, and identified each $\mathcal{E}_{\text{spam}}$ as the noise contribution to SPAM; in the penultimate line (purely for notational reasons) we defined $\phi(W) := \mathcal{E}'_{\text{spam}_w} \mathcal{U}'_W$ and in the last line, $\mathcal{U}_W = \mathcal{U}'_W$ and $\mathcal{E}_{\text{spam}_w} = \mathcal{E}'_{\text{spam}_w}$.

Putting this together with the probability of getting another n -bit string \mathbf{s}' with the same layer sequence,

$$\begin{aligned}
P_{1,C}(\mathbf{s})P_{1,C}(\mathbf{s}') &= \mathbb{E}_{\substack{L_1 \sim \Omega \\ \psi \sim \Omega_1}} \langle \mathbf{s} | \mathcal{U}_W \mathcal{E}_{\text{spam}_w} \mathcal{E}_1 \mathcal{U}_1 \mathcal{E}_{\text{spam}_v}(|\psi\rangle\langle\psi|) | \mathbf{s} \rangle \langle \mathbf{s}' | \mathcal{U}_W \mathcal{E}_{\text{spam}_w} \mathcal{E}_1 \mathcal{U}_1 \mathcal{E}_{\text{spam}_v}(|\psi\rangle\langle\psi|) | \mathbf{s}' \rangle \\
&= \mathbb{E}_{\substack{L_1 \sim \Omega \\ \psi \sim \Omega_1}} \langle \mathbf{s} | \mathcal{U}_W \mathcal{E}_{\text{spam}_w} \mathcal{E}_1 \mathcal{U}_1 \mathcal{E}_{\text{spam}_v} [|\psi\rangle\langle\psi| \mathcal{E}_{\text{spam}_v}^\dagger \mathcal{U}_1^\dagger \mathcal{E}_1^\dagger \mathcal{E}_{\text{spam}_w}^\dagger \mathcal{U}_W^\dagger (|\mathbf{s}'\rangle\langle\mathbf{s}'|) |\psi\rangle\langle\psi|] | \mathbf{s} \rangle \\
&= \mathbb{E}_{\substack{L_1 \sim \Omega \\ \psi \sim \Omega_1}} \langle \mathbf{s} | \mathcal{U}_W \mathcal{E}_{\text{spam}_w} \mathcal{E}_1 \mathcal{U}_1 \mathcal{E}_{\text{spam}_v} \mathcal{P}_\psi \mathcal{E}_{\text{spam}_v}^\dagger \mathcal{U}_1^\dagger \mathcal{E}_1^\dagger \mathcal{E}_{\text{spam}_w}^\dagger \mathcal{U}_W^\dagger (|\mathbf{s}'\rangle\langle\mathbf{s}'|) | \mathbf{s} \rangle, \tag{49}
\end{aligned}$$

where in the last line we defined $\mathcal{P}_\psi(\cdot) := |\psi\rangle\langle\psi| \cdot |\psi\rangle\langle\psi|$.

Now we can exploit the identity derived in [67],

$$F_{\text{ent}}(\mathcal{X}) = \sum_x (-2)^{-h(x,y)} \langle x | \mathbb{E}_{U_i \sim \text{Haar}} \left\{ \mathcal{U}_U^\dagger \mathcal{X} \mathcal{U}_U \right\} [|y\rangle\langle y|] | x \rangle, \tag{50}$$

where here F_{ent} is entanglement fidelity, defined in Eq. (31), and \mathcal{U}_U is the noiseless unitary map corresponding to the product $U = \otimes_{i=1}^n U_i$ with local, single-qubit random unitaries U_i . Since this expression requires two copies of \mathcal{U}_U , where only the individual U_i should be Haar random, it suffices for these (as opposed to the global unitary) to belong to a unitary 2-design, e.g., the single-qubit Clifford group.

We emphasize then, that we will require the RMs to be randomized by a layer made up of uniformly random single-qubit Clifford gates; while in the main text we fix this to correspond to \mathbb{G}_1 and Ω_1 , all

other layers in principle can be chosen arbitrarily (with the reasoning of having some better choices than others detailed in the previous sections).

We can now apply Eq. (50) on Eq. (49), so that

$$\begin{aligned} \text{tr}(\tilde{\varrho}_1^2) &\simeq 4^n \mathbb{E}_{\substack{L_1 \sim \Omega \\ \psi \sim \Omega_1}} F_{\text{ent}}(\mathcal{E}_{\text{spam}_w} \mathcal{E}_1 \mathcal{U}_1 \mathcal{E}_{\text{spam}_v} \mathcal{P}_\psi \mathcal{E}_{\text{spam}_v}^\dagger \mathcal{U}_1^\dagger \mathcal{E}_1^\dagger \mathcal{E}_{\text{spam}_w}^\dagger) \\ &= \mathbb{E}_{\substack{L_1 \sim \Omega \\ \psi \sim \Omega_1}} F_\psi(\mathcal{E}_{\text{spam}_v}^\dagger \mathcal{U}_1^\dagger \mathcal{E}_1^\dagger \mathcal{E}_{\text{spam}_w}^\dagger \mathcal{E}_{\text{spam}_w} \mathcal{E}_1 \mathcal{U}_1 \mathcal{E}_{\text{spam}_v}), \end{aligned} \quad (51)$$

where the second line follows directly from the definition of entanglement fidelity. This generalizes to any circuit depth m , to

$$\text{tr}(\tilde{\varrho}_m^2) = \mathbb{E}_{\substack{L_i \sim \Omega \\ \psi \sim \Omega_1}} F_\psi(\mathcal{E}_{\text{spam}_v}^\dagger \mathcal{U}_1^\dagger \mathcal{E}_1^\dagger \cdots \mathcal{U}_m^\dagger \mathcal{E}_m^\dagger \mathcal{E}_{\text{spam}_w}^\dagger \mathcal{E}_{\text{spam}_w} \mathcal{E}_m \mathcal{U}_m \cdots \mathcal{E}_1 \mathcal{U}_1 \mathcal{E}_{\text{spam}_v}), \quad (52)$$

which coincides with Eq. (40) up to $\mathcal{E}_{\text{spam}_w}$.

Now similar to point 3 in § B.4 above, we mainly care about an exponential decay, which occurs for Ω -distributed circuits being an approximate unitary 2-design and noise being approximately gate+time independent, unital and TP. Now we will have

$$\text{tr}(\tilde{\varrho}_m^2) \approx A u(\tilde{\Xi}_p)^m + \frac{1}{2^n}, \quad (53)$$

for $A = 2^{-n}(2^n - 1)u(\tilde{\Xi}_{q_{\text{spam}_w}})\mathbb{E}_{\psi \sim \Omega_1} u_\psi(\mathcal{E}_{\text{spam}_v})$, where $\tilde{\Xi}_{q_{\text{spam}_w}}$ is the contribution from the layer average of $\mathcal{E}_{\text{spam}_w}$; of course both unitarity terms in A cannot be distinguished and can simply be interpreted as an average unitarity of SPAM.

The result in Eq. (53) corresponds to that with an exact average over layers and initial states; this average can be approximated numerically with Eq. (11) given a number N_W of measurements, C_m of Ω -distributed circuits, and N_V of initial randomization samples, respectively.

D Operational estimation of fidelity through randomized measurements

Since estimating the average unitarity is really useful only when informed by the average fidelity, we now consider estimating the average layer fidelity of the same Ω -distributed circuits, once given a set of randomized measurement probabilities P_U .

Naturally, if the noiseless output is a state $|\varphi\rangle$, Eq. (46) can be modified to account for its fidelity with respect to a mixed state ρ as

$$\langle \varphi | \rho | \varphi \rangle = 2^n \sum_{\mathbf{s}, \mathbf{s}_{\text{ideal}}} (-2)^{-h(\mathbf{s}, \mathbf{s}_{\text{ideal}})} \mathbb{E}_{U \sim \text{Haar}} P_U(\mathbf{s}) P_U^{(\text{ideal})}(\mathbf{s}_{\text{ideal}}), \quad (54)$$

where $P_U^{(\text{ideal})}$ is the probability of observing a n -bit string $\mathbf{s}_{\text{ideal}}$ with a randomized measurement defined by U on $|\varphi\rangle\langle\varphi|$, that is

$$P_U^{(\text{ideal})}(\mathbf{s}_{\text{ideal}}) = |\langle \mathbf{s}_{\text{ideal}} | U | \varphi \rangle|^2. \quad (55)$$

Notice that this assumes that we can efficiently compute the n -bit strings, and thus the probabilities, corresponding to the noiseless outputs. This generally implies a limitation in the gate sets that can be employed to only Clifford gates, however, for mid-scale estimations the ideal probabilities can still be computed without a major overhead when the gate set contains non-Clifford gates to be sampled with a relatively low probability.

In our case, we want to estimate the quantity $\langle \psi_m | \tilde{\rho}_m | \psi_m \rangle$, where

$$\begin{aligned} |\psi_m\rangle\langle\psi_m| &:= \mathbf{C}_m^{(\text{ideal})}(|0\rangle\langle 0|) = \mathcal{U}_m \cdots \mathcal{U}_1 \mathcal{U}_V (|0\rangle\langle 0|) \\ &= \mathcal{U}_m \cdots \mathcal{U}_1 (|\psi\rangle\langle\psi|). \end{aligned} \quad (56)$$

Thus, consider first the case $m = 1$; we have

$$\mathbf{P}_{1,W}(\mathbf{s}) \mathbf{P}_{1,W}^{(\text{ideal})}(\mathbf{s}_{\text{ideal}}) = \mathbb{E}_{\substack{\mathbf{L}_1 \sim \Omega \\ \psi \sim \Omega_1}} \langle \mathbf{s} | \mathcal{U}_W \mathcal{E}_{\text{spam}_w} \mathcal{E}_1 \mathcal{U}_1 \mathcal{E}_{\text{spam}_v} \mathcal{P}_\psi \mathcal{U}_1^\dagger \mathcal{U}_W^\dagger (|\mathbf{s}_{\text{ideal}}\rangle\langle\mathbf{s}_{\text{ideal}}|) | \mathbf{s} \rangle, \quad (57)$$

which follows as in Eq. (49), where in the last line we defined $\mathcal{P}_\psi(\cdot) := |\psi\rangle\langle\psi| \cdot |\psi\rangle\langle\psi|$. Similarly, we can follow all steps from Eq. (49) to Eq. (52) in an analogous way to obtain

$$\langle \psi_m | \tilde{\rho}_m | \psi_m \rangle = \mathbb{E}_{\substack{\mathbf{L}_i \sim \Omega \\ \psi \sim \Omega_1}} \mathbf{F}_\psi(\mathcal{U}_1^\dagger \cdots \mathcal{U}_m^\dagger \mathcal{E}_{\text{spam}_w} \mathcal{E}_m \mathcal{U}_m \cdots \mathcal{E}_1 \mathcal{U}_1 \mathcal{E}_{\text{spam}_v}), \quad (58)$$

which is simply an Randomized Benchmarking (RB)-like fidelity decay. Similarly here, if the Ω -distributed circuits approximate a unitary 2-design, to the effect that $\mathbb{E}_{\mathbf{L} \sim \Omega} \mathcal{U}_L^\dagger \mathcal{E}_i \mathcal{U}_L \approx \tilde{\Xi}_{p_i}$, i.e., the average noise is approximately a global depolarizing channel with $p_i = (2^n \bar{\mathbf{F}}(\mathcal{E}) - 1)/(2^n - 1)$, we end up with

$$\begin{aligned} \langle \psi_m | \tilde{\rho}_m | \psi_m \rangle &\approx \mathbb{E}_{\psi \sim \Omega_1} \mathbf{F}_\psi(\tilde{\Xi}_{p'_m} \tilde{\Xi}_{p_{m-1}} \cdots \tilde{\Xi}_{p_1} \mathcal{E}_{\text{spam}_v}) \\ &= \mathbb{E}_{\psi \sim \Omega_1} \mathbf{F}_\psi(\tilde{\Xi}_{p_{\text{spam}_w}} \tilde{\Xi}_{p_m p_{m-1} \cdots p_1} \mathcal{E}_{\text{spam}_v}), \end{aligned} \quad (59)$$

which is a RB-like decay of the state fidelity in the circuit depth m , where we defined $p'_m = p_m p_{\text{spam}_w}$ for some p_{spam_w} . Further, for time-independent noise, such that $p_1 = p_2 = \dots = p_m = p$, this is an exponential decay in m ,

$$\langle \psi_m | \tilde{\rho}_m | \psi_m \rangle \approx A p^m + B, \quad (60)$$

where $A = p_{\text{spam}_w} [\mathbf{F}_\psi(\mathcal{E}_{\text{spam}_v}) - 2^{-n}]$, $B = 2^{-n}$, and

$$p = \frac{2^n \bar{\mathbf{F}}(\mathcal{E}) - 1}{2^n - 1}, \quad (61)$$

which can similarly be written in terms of entanglement fidelity of \mathcal{E} , or in terms of its matrix representation, similar to the usual RB constants for unital SPAM.

This means we can generate a set of random Ω -distributed circuits, attach some set of randomized measurements, and use the probabilities to simultaneously estimate average layer fidelity and unitarity.

E Scrambling and unitary 2-designs

Here we refer to both assumptions, [A₁](#), [A₂](#), as written in the main text in § 4.1.1, for an exponential decay of the average sequence purity in circuit depth.

While assumption [A₁](#) is beyond the choices that the user executing the protocol 4.1 can make, assumption [A₂](#) is important to make the protocol 3 adhere to the exponential decay of main Result 2, but it also sets a practical limit in scalability to mid-scale systems, which we discuss below.

There is, furthermore, a fundamental limit to scalability imposed by the *sample complexity* of estimating purity via RMs, i.e., the number of experimental samples, N_{meas} in Eq. (10), needed to estimate purity within a given error. This is discussed in the main text in § 6.1, and it compounds with the sample complexity of the Ω -distributed circuits, related to assumption [A₂](#).

The need for unitary 2-designs in RB-based techniques stems from the fact that, by definition, these inherit the property of fully random (i.e. Haar distributed) unitaries whereby their second moment is described by a depolarizing channel, which requires a single parameter to be fully specified. This implies that figures of merit, such as average gate fidelity or average gate unitarity can be encapsulated into such polarization parameter (once assumption [A₁](#) is satisfied) given circuits that generate a unitary 2-design.

Loosely speaking, a unitary 2-design is a probability distribution μ on the unitary group, or a subset thereof, satisfying $\mathbb{E}_{V \sim \mu} \mathcal{V}^\dagger \mathcal{X} \mathcal{V} = \mathbb{E}_{U \sim \text{Haar}} U^\dagger \mathcal{X} U$ for any quantum channel \mathcal{X} . The action $\mathbb{E}_{V \sim \mu} \mathcal{V}^\dagger(\cdot) \mathcal{V}$ is referred to as a 2-twirl with μ . That is, the 2-twirl with μ reproduces the second moment of the whole unitary group with the Haar measure. That an ensemble of unitaries constitutes a 2-design is particularly useful because it is known that doing a 2-twirl with the Haar measure on a CP map, reduces it to a depolarizing channel [\[65\]](#), i.e., also for a 2-design $\mathbb{E}_{V \sim \mu} \mathcal{V}^\dagger \mathcal{X} \mathcal{V}(\cdot) = p(\cdot) + (1-p)\mathbb{1}/2^n$, where here $p = (2^n \bar{F}(\mathcal{X}) - 1)/(2^n - 1)$, where $\bar{F}(\mathcal{X})$ is the average gate fidelity of \mathcal{X} . Both [Eq. \(14\)](#) and [Eq. \(3\)](#) are obtained using this relation.

The notion of a unitary 2-design can further be relaxed by having equality up to a small ϵ according to a given metric, to the effect that the 2-twirl is also *close* to a depolarizing channel. More precisely, denoting a 2-twirl by $\Delta_\mu(\cdot) := \mathbb{E}_{V \sim \mu} \mathcal{V}^\dagger(\cdot) \mathcal{V}$ we say that \mathbb{V} is an ϵ -approximate unitary 2-design, if

$$(1 - \epsilon)\Delta_{\text{Haar}} \preceq \Delta_\mu \preceq (1 + \epsilon)\Delta_{\text{Haar}}, \quad (62)$$

where here \preceq is semidefinite ordering in the sense that $\mathcal{X} \preceq \mathcal{Y}$ if and only if $\mathcal{X} - \mathcal{Y}$ is a CP map. This definition was put forth (for the more general setting of t -designs) in [\[63\]](#) and has the particularly simple interpretation of having a small multiplicative factor $1 \pm \epsilon$ of difference when measuring a state acted on with a channel twirled Δ_μ as opposed to with Δ_{Haar} ¹¹. Thus, the approximation sign in both [Eq. \(13\)](#) and [Eq. \(15\)](#) refers to these small multiplicative factors in the 2-design approximation, exponential in m .

A well-known example of an exact 2-design is the n -qubit Clifford group [\[46\]](#): it is also simultaneously a strong reason why standard¹² Clifford RB works so well, and the culprit (in practice) of why it does not scale in n . Techniques akin to standard Clifford RB, such as Direct Randomized Benchmarking (DRB), Mirror Randomized Benchmarking (MRB) and Binary Randomized Benchmarking (BiRB) resolve such scalability issues by, among other things, retaining some of the randomness through Ω -distributed circuits. Rather than requiring an approximate unitary design property, e.g., MRB [\[22\]](#) and BiRB [\[23\]](#) require a scrambling property in the sense that Pauli errors get quickly spread among other qubits before other Pauli errors occur. This can be stated in terms of an entanglement fidelity for non-identity Paulis P, P' , with action $\mathcal{P}(\cdot) = P(\cdot)P$ and $\mathcal{P}'(\cdot) = P'(\cdot)P'$, such that for an expected infidelity of the layers α , there is $k \ll 1/\alpha$ and a $\delta \ll 1$ with

$$\mathbb{E}_\Omega F_{\text{ent}}[\mathcal{P} \mathcal{C}_\Omega \mathcal{P}' \mathcal{C}_\Omega^{-1}] \leq \delta + \frac{1}{4^n}, \quad (63)$$

where here $\mathcal{C}_\Omega = \mathcal{U}(\mathbb{L}_k \cdots \mathbb{L}_1)$, with \mathcal{U} the unitary map of the sequence of noiseless layers $\mathbb{L}_k \cdots \mathbb{L}_1$. Similarly, DRB uses *generators* of unitary 2-designs as the benchmarking gate set and then requires that these constitute a *sequence-asymptotic* unitary 2-design [\[51\]](#).

While the scrambling condition in [Eq. \(63\)](#) is stated for Pauli noise channels, the choice of (\mathbb{G}_1, Ω_1) being the uniformly distributed single-qubit Clifford group has the effect of projecting any CP map (modeling Markovian noise) to a Pauli channel (i.e., a tensor product of depolarizing channels) since each Clifford group constitutes a unitary 2-design on the respective qubit.

¹¹This definition is further connected in [\[63\]](#) to the usual diamond norm definition as implying that if \mathbb{V} is an ϵ -approximate unitary 2-design, also $\|\Delta_\mu - \Delta_{\text{Haar}}\|_\diamond \leq 2\epsilon$, where $\|\mathcal{X}\|_\diamond := \sup_\rho \|(\mathcal{I}_d \otimes \mathcal{X})\rho\|_1$, where $\|X\|_1 = \text{tr} \sqrt{X X^\dagger}$ denotes trace norm and the supremum is taken over all dimensions $d \geq 1$ of the identity and corresponding density matrices ρ .

¹²As can be seen in [\[20\]](#) and [\[68\]](#), there is a plethora of techniques under the term RB; by standard we mean single or two-qubit RB with corresponding Clifford gate sets, estimating the group's average gate fidelity by fitting survival probabilities to an exponential decay in sequence length.

The reason approximating a unitary 2-design is a stronger condition than scrambling, as defined by Eq. (63), is because it would require δ shrinking as $\mathcal{O}(4^{-n})$ ¹³. Nevertheless, while we directly assume that our Ω -distributed circuits approximate a unitary 2-design, for a mid-scale of tenths of qubits the scrambling condition suffices, and indeed it holds in a similar way than it does in MRB or BiRB¹⁴, as exemplified in § 5. Increasing the qubit count to estimate average unitarity would require establishing a scrambling condition, e.g., as for BiRB by employing stabilizer states and measurements, or otherwise relaxing the approximate design condition.

F Numerical addendum

F.1 The simulator backend

As explained in the main text in § 5, we performed experiments on IQM SparkTM, a 5-qubit superconducting system with a central qubit connected to the rest, and simulations with a backend of a total of 20 qubits in a grid topology, connected as depicted in the graph of Fig. 7. In the simulation, we considered a subset of these qubits, namely qubits ranging from qubit 3 to qubit 12, in pairs as depicted in Fig. 8(b). All qubits were associated with a noise model on readout, gate times, single- and two-qubit depolarizing noise, and decoherence, T_1 and T_2 times.

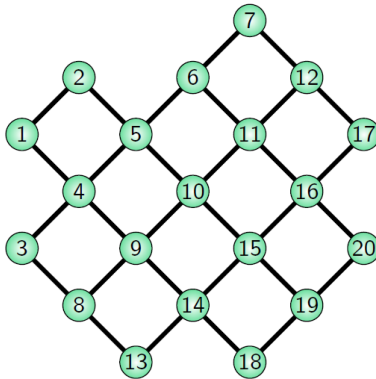


Figure 7: **Backend topology and connectivity:** We consider a backend with 20 possible qubits (circles), with each qubit labeled with a given integer and connected to another as depicted by the corresponding edges. We employ Ω -distributed circuits with only single- and two-qubit gates, with two-qubits gates acting only between pairs of connected qubits.

F.2 Simulation on 10 qubits

We now employ a simulator backend that considers 20 possible qubits with a grid topology, as displayed fully in Fig. 7 of Appendix F.1. All operations (except barriers) are modeled as noisy, in this particular example with a set of parameters considering a range of relaxation times T_1 , dephasing times T_2 , gate duration parameters, depolarizing parameters on both single- and two-qubit gates, and readout errors (bit-flip probabilities).

Similarly in this case, according to Protocol 4.1, we extracted decay rates of the average state purity and fidelity in increasing depths, and thus average layer unitarity and fidelity for Ω -distributed circuits with up to 10 qubits. In Fig. 8, we show the corresponding purity decays in increasing depth. We display only even qubit numbers n for easiness of visualization, where each n corresponds to choices of

¹³This can be seen e.g., by assuming the $\mathcal{U}(L_k \cdots L_1)$ generates a unitary 2-design and using Eq. (32)

¹⁴A difference of our technique with MRB is that we do not employ a mirror structure, while one with BiRB is that we do not employ initial and final stabilizers.

Purity decays with 10 random circuits and 10 RMs
 Gate set: \mathcal{G}_1 =Clifford, $\mathcal{G}_2:\Omega_2=\{\text{CZ}: 1\}$; 2Q gate density: 0.5
 Backend: Fake grid backend (20 qubits)

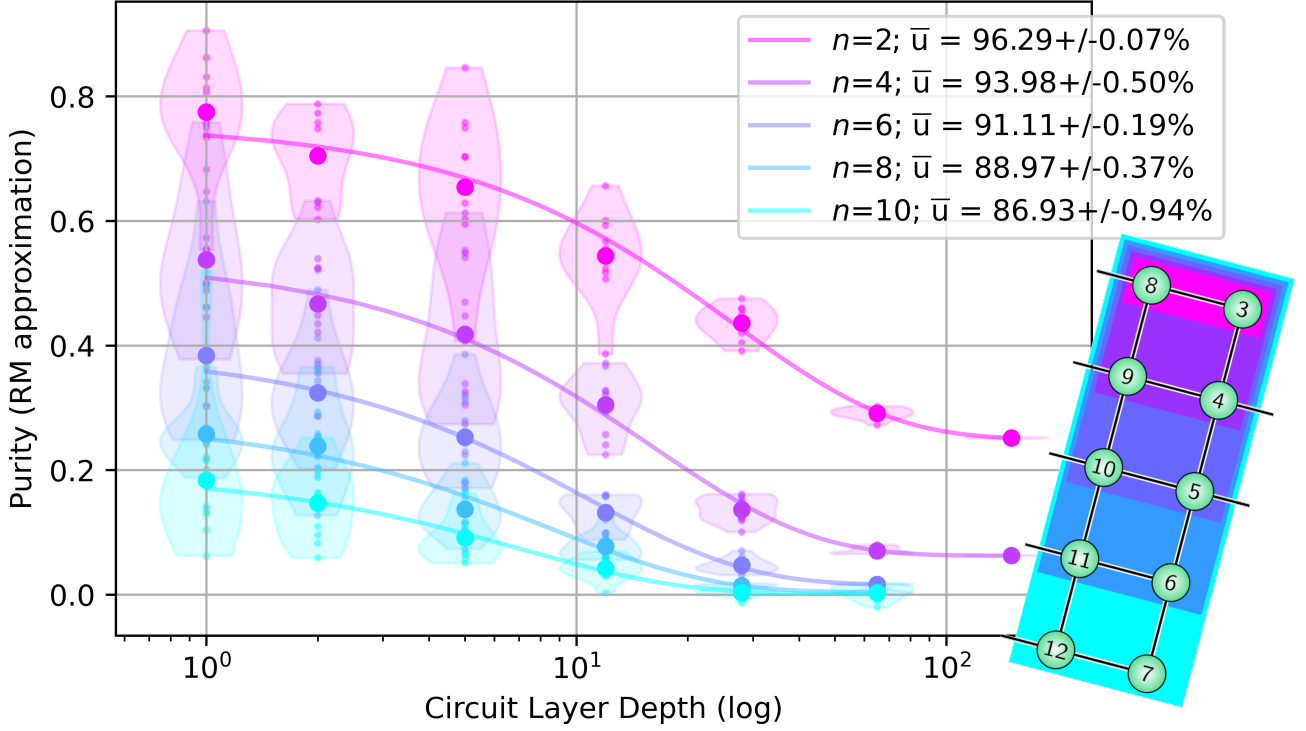


Figure 8: **Purity decays for simulated backend.** Numerical simulation for purity decays computed according to Protocol 4.1 for Ω -distributed circuits using the gate set $\mathcal{G} = \text{Clif}_1 \cup \{\text{CZ}\}$, with Clif_1 being the uniformly-distributed single-qubit Clifford group. Individual plots correspond to a given number of qubits n , taken from a connectivity graph shown in (b), whereby smaller points correspond to Median of Means (MoMs) estimators of purity with Eq. (11) at a given depth m , bigger points correspond to the average purity, violins show the distribution of the MoMs estimators, and lines correspond to a least-squares fit of the averages to the decay model in Eq. (13), whereby the average unitarities \bar{u} in corresponding number of qubits n are estimated. Sample parameters: $N_{C_m^*} = 12$, $N_W = 9$, $N_{\text{meas}} = 2^{10}$ and $K = 9$ MoMs.

qubits and couplings as shown in the inset. In all cases, we employed unbiased estimators and $K = 2$ Median of Means (MoMs) estimators.

In Fig. 9 we show all average layer fidelities and unitarities in increasing number of qubits, together with the Pauli noise unitarity intervals as predicted by the bound in Ineq. (4). In the corresponding inset, we show the average state fidelity decays in increasing depth for each number of qubits n , and thus the corresponding average gate fidelities; similar to the case of IQM SparkTM, these were computed using the measurements within the same experiment and using the estimator in Eq. (12) using the measurements of the noiseless circuits. The noiseless probabilities were estimated with the same number of $N_{\text{meas}} = 2^{10}$ shots per measurement.

Generally, while variances in the decays are relatively high, the averages show only a modest deviation up to 9 qubits. The noise model is dominated by stochastic errors, so it is expected that most points should fall within the Pauli unitarity bound; the cases of $n = 6, 8$ are indeed outliers, which in experiment would need to be investigated further, in our case they most likely can be explained by both the qubit arrangement and the amplitude damping T_1 parameters involved. It should be noted that for simulation in a common laptop, going beyond 10 qubits becomes quite computationally demanding.

Avg layer fidelity and unitarity for 12 random circuits and 9 RMs
 Gate set: \mathcal{G}_1 =Clifford, $\mathcal{G}_2:\Omega_2=\{\text{CZ}: 1\}$; 2Q gate density: 0.5
 Backend: Fake grid backend (20 qubits)

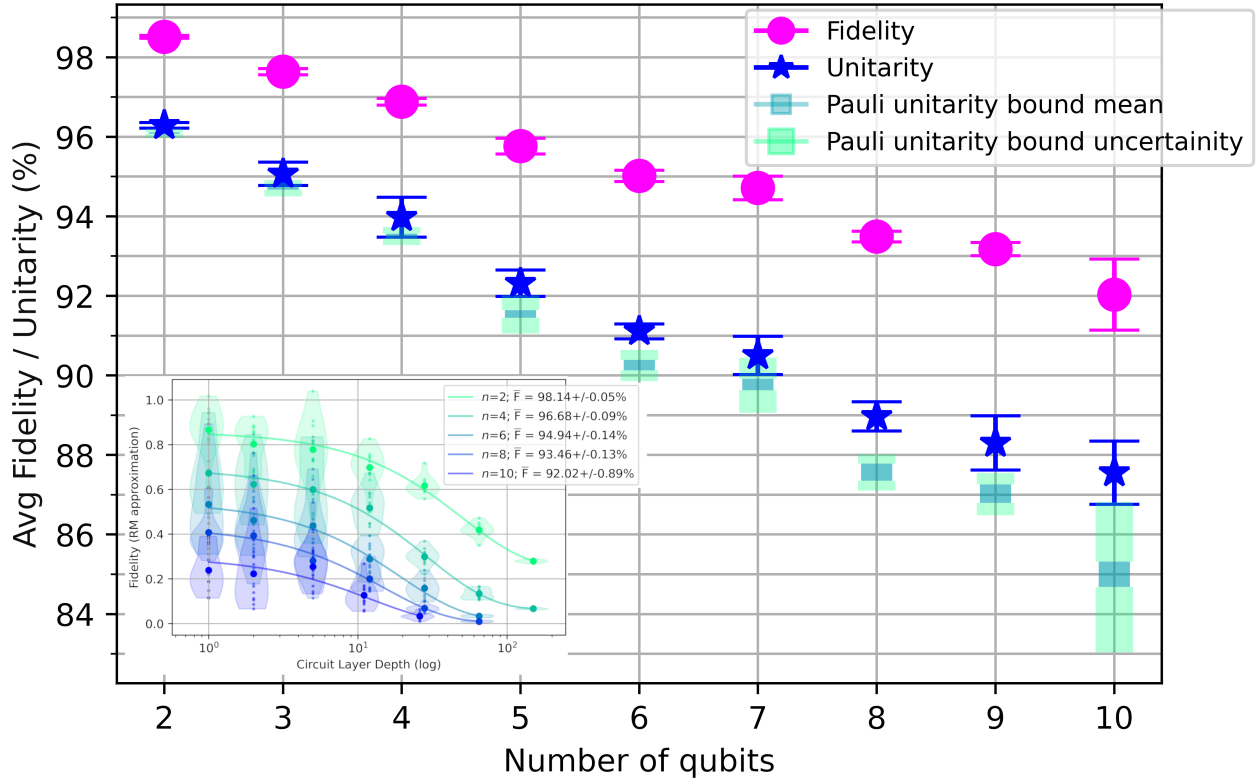


Figure 9: **Average layer fidelities and unitarities in number of qubits for simulated backend.** Qubit layouts correspond to those of the inset of Fig. 8 (for odd n , the smaller qubit label was taken); data corresponding to the same Ω -distributed circuits with gate ensemble $\mathcal{G} = \text{Clif}_1 \cup \{\text{CZ}\}$. In the inset, we show corresponding fidelity decays for even n , where individual plots correspond to a given number of qubits, small points to Median of Means (MoMs) estimators of Eq. (12) at given depths, larger points to the respective average purity, and lines to least-squares fit of the averages to the model in Eq. (15), whereby the corresponding average layer fidelity \bar{F} for respective n is extracted according to Eq. (3). Sample parameters: $N_{C_m} = 12$, $N_W = 9$, $N_{\text{meas}} = 2^{10}$ and $K = 9$ MoMs. Pauli unitarity bounds computed according to Ineq. (4).

F.3 Comparison of layer fidelity estimations with MRB

The Ω -distributed circuits we consider are a primitive component in MRB [22], thus the average fidelity estimations from both our technique and MRB should agree. There are two main differences between both procedures: one is that we do not construct a “mirror” circuit, i.e., we do not append the circuit made up of the inverses of the original Ω -distributed circuit, and the second is that we do not interleave layers of random Pauli gates. Our technique is able to estimate average unitarity too, although this comes at a sampling complexity cost that requires exponentially many more samples to increase accuracy.

F.3.1 IQM Spark™

The estimated fidelities from randomized measurements should be consistent with those estimated by MRB [22]. Indeed, a primitive of MRB is Ω -distributed circuits; a difference with our technique is that we do not implement a mirror (i.e. the sequence of inverses), nor interleave random Pauli operators. Nevertheless, both techniques can estimate the same quantity (MRB through polarizations instead of

state fidelities), RMs simply enable to access the unitarity. In Fig. 10 we show the fidelity decays obtained experimentally with MRB about a month ago on IQM SparkTM, with the same Ω -distributed circuits considered in § 5, namely made up of single-qubit Clifford gates uniformly sampled and CZ gates with a two-qubit gate density of 1/2 according to the edge-grab sampler.

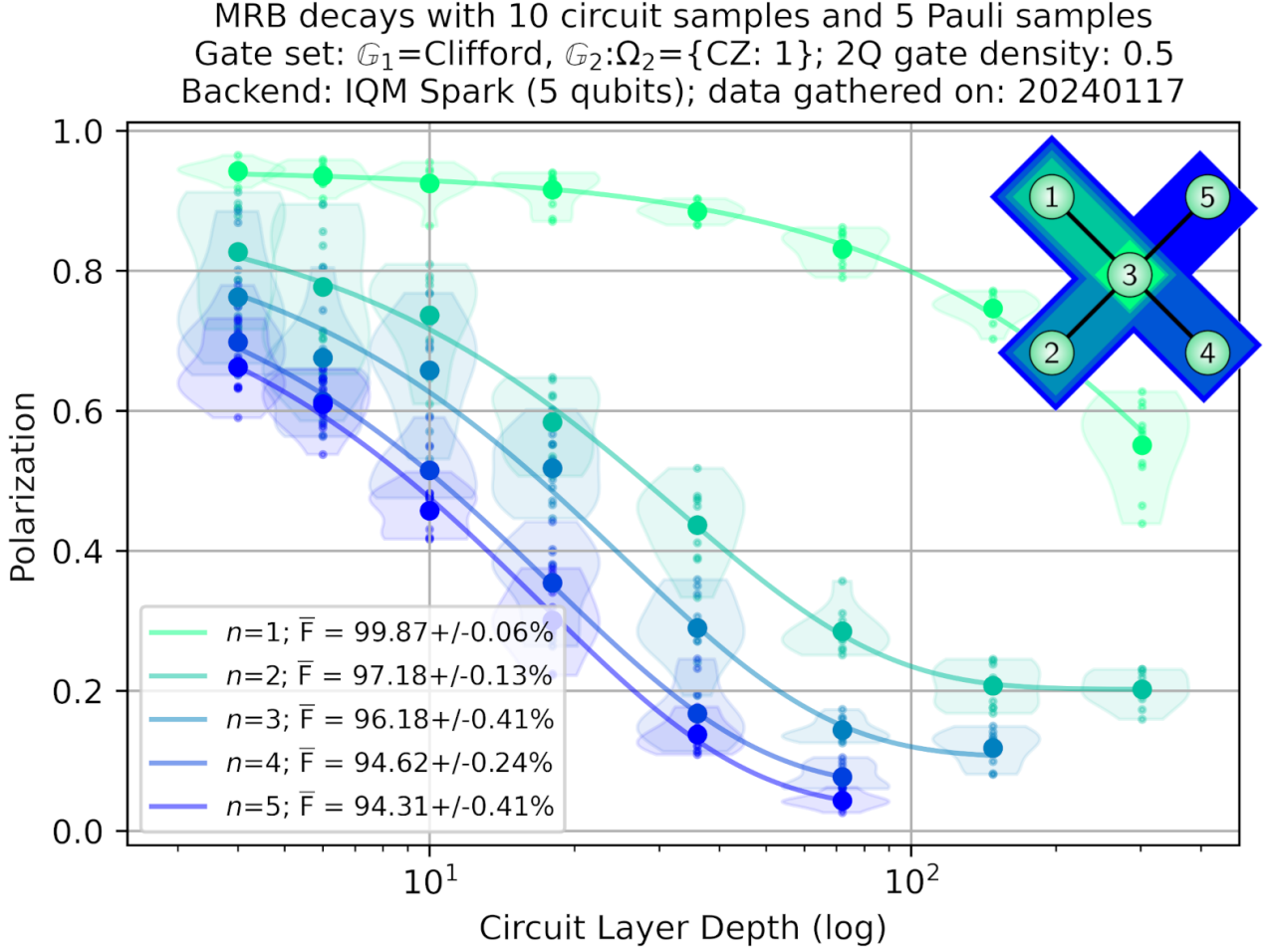


Figure 10: **Comparison with MRB on IQM SparkTM**: For the same Ω -distributed circuits considered in § 5

Clearly, while the estimated average layer fidelities agree, the distributions have a smaller variance than those in Fig. 5, and were obtained with less total circuit samples. It can be conceivable then, that alternatively, average fidelities may be computed by constructing mirror circuits and following the MRB protocol [22], at the expense of performing separate measurements of these circuits.

G Unitarity and randomized compiling

To begin with, let us label the n -qubit Pauli group \mathbb{P}_n , i.e., the group made up of all n -fold products of Pauli operators ($\mathbf{1}, X, Y, Z$), as in [69]: let \mathbf{a} be a $2n$ -bit string, $\mathbf{a} = a_1 a_2 \dots a_{2n}$, and define

$$P_{\mathbf{a}} := i^{\mathbf{a}^T \Upsilon \mathbf{a}} \prod_{j=1}^n X_j^{a_{2j-1}} Z_j^{a_{2j}}, \quad (64)$$

where X_j and Z_j are single-qubit Pauli operators acting on the j^{th} qubit and $\Upsilon := \oplus_{j=1}^n \begin{pmatrix} 0 & 1 \\ 0 & 0 \end{pmatrix}$ such that $P_{\mathbf{a}}$ is ensured to be Hermitian. The Pauli group \mathbb{P}_n is then made up of all such $P_{\mathbf{a}}$ together with

their products and their overall phases $\{\pm 1, \pm i\}$; e.g., $\mathbb{P}_1 = \{\pm \mathbb{1}, \pm i\mathbb{1}, \pm X, \dots, \pm iZ\}$. In particular, denoting any other $2n$ -bit strings with bold lowercase letters, we will make use of the property

$$P_{\mathbf{a}}P_{\mathbf{b}} = (-1)^{\langle \mathbf{a}, \mathbf{b} \rangle} P_{\mathbf{b}}P_{\mathbf{a}}, \quad (65)$$

where

$$\begin{aligned} \langle \mathbf{a}, \mathbf{b} \rangle &:= \mathbf{a}^T(\Upsilon + \Upsilon^T)\mathbf{b} \pmod{2} \\ &= (a_1b_2 + a_2b_1 + a_3b_4 + a_4b_3 + \dots + a_{2n}b_{2n-1} + a_{2n-1}b_{2n}) \pmod{2}, \end{aligned} \quad (66)$$

which in particular is such that

$$\frac{1}{4^n} \sum_{\mathbf{a}} (-1)^{\langle \mathbf{a}, \mathbf{b} + \mathbf{c} \rangle} = \delta_{\mathbf{b}\mathbf{c}}. \quad (67)$$

Let us then write a generic n -qubit noise channel (i.e., some CP map) in the so-called χ -representation, $\mathcal{E}(\cdot) = \sum_{\mathbf{a}, \mathbf{b}} \chi_{\mathbf{a}\mathbf{b}} P_{\mathbf{a}}(\cdot)P_{\mathbf{b}}$, where χ is a positive Hermitian matrix. We can also relate this representation to the so-called Pauli Transfer Matrix (PTM) representation, which is a 4^n -square matrix with real entries given by

$$\begin{aligned} \mathcal{E}_{\mathbf{a}\mathbf{b}} &:= \frac{1}{2^n} \text{tr}[P_{\mathbf{a}}\mathcal{E}(P_{\mathbf{b}})] \\ &= \frac{1}{2^n} \sum \chi_{\mathbf{c}\mathbf{d}} \text{tr}[P_{\mathbf{a}}P_{\mathbf{c}}P_{\mathbf{b}}P_{\mathbf{d}}], \end{aligned} \quad (68)$$

which is not quite informative by itself; however, a particular case where this representation is useful is for the case of a Pauli channel, which has for χ a diagonal matrix, implying that its PTM is diagonal too. A Pauli channel can be enforced on any channel by twirling it with the Pauli group, i.e.,

$$\mathcal{E} \mapsto \mathcal{E}^{\circlearrowleft}(\cdot) := \frac{1}{4^n} \sum_{P \in \mathbb{P}_n} P\mathcal{E}(P \cdot P)P, \quad (69)$$

which gives

$$\begin{aligned} \mathcal{E}_{\mathbf{a}\mathbf{b}}^{\circlearrowleft} &= \frac{1}{2^{3n}} \sum_{\mathbf{c}, \mathbf{d}, \mathbf{q}} \chi_{\mathbf{c}\mathbf{d}} \text{tr}[P_{\mathbf{a}}P_{\mathbf{q}}P_{\mathbf{c}}P_{\mathbf{q}}P_{\mathbf{b}}P_{\mathbf{q}}P_{\mathbf{d}}P_{\mathbf{q}}] \\ &= \frac{1}{2^{3n}} \sum_{\mathbf{c}, \mathbf{d}, \mathbf{q}} (-1)^{\langle \mathbf{q}, \mathbf{c} + \mathbf{d} \rangle} \chi_{\mathbf{c}\mathbf{d}} \text{tr}[P_{\mathbf{a}}P_{\mathbf{c}}P_{\mathbf{b}}P_{\mathbf{d}}] \\ &= \frac{1}{2^n} \sum_{\mathbf{c}, \mathbf{d}} \chi_{\mathbf{c}\mathbf{d}} \delta_{\mathbf{c}\mathbf{d}} \text{tr}[P_{\mathbf{a}}P_{\mathbf{c}}P_{\mathbf{b}}P_{\mathbf{d}}] \\ &= \frac{1}{2^n} \sum_{\mathbf{d}} \chi_{\mathbf{d}\mathbf{d}} \text{tr}[P_{\mathbf{a}}P_{\mathbf{d}}P_{\mathbf{b}}P_{\mathbf{d}}] \\ &= \delta_{\mathbf{a}\mathbf{b}} \sum_{\mathbf{d}} (-1)^{\langle \mathbf{a}, \mathbf{d} \rangle} \chi_{\mathbf{d}\mathbf{d}} := \delta_{\mathbf{a}\mathbf{b}} \sum_{\mathbf{d}} (-1)^{\langle \mathbf{a}, \mathbf{d} \rangle} \alpha_{\mathbf{d}}, \end{aligned} \quad (70)$$

where we made use of both Eq. (65) and Eq. (67), so that indeed $\mathcal{E}^{\circlearrowleft}$, the PTM of the twirled map $\mathcal{E}^{\circlearrowleft}$, is manifestly diagonal with eigenvalues $\lambda_{\mathbf{a}} := \sum_{\mathbf{b}} (-1)^{\langle \mathbf{a}, \mathbf{b} \rangle} \alpha_{\mathbf{b}}$, where we write the diagonal elements with a single index as $\alpha_{\mathbf{a}} := \chi_{\mathbf{a}\mathbf{a}}$.

The diagonal elements α are the so-called Pauli error probability rates, conversely related to the PTM eigenvalues as $\alpha_{\mathbf{a}} = 2^{-n} \sum_{\mathbf{b}} (-1)^{\langle \mathbf{a}, \mathbf{b} \rangle} \lambda_{\mathbf{b}}$, and in terms of these, the trace non-increasing condition translates to $\sum_{\mathbf{a}} \alpha_{\mathbf{a}} \leq 1$, saturating for \mathcal{E} being TP.

It follows that the average gate fidelity of a Pauli channel is given by

$$\begin{aligned}
\bar{F}(\mathcal{E}^\odot) &= \frac{\text{tr}[\mathcal{E}^\odot] + 2^n}{2^n(2^n + 1)} \\
&= \frac{\sum_{\mathbf{a}} \lambda_{\mathbf{a}} + 2^n}{2^n(2^n + 1)} \\
&= \frac{2^n \alpha_{\mathbf{0}} + 1}{2^n + 1} \\
&= \bar{F}(\mathcal{E}) \\
\mathcal{E} \stackrel{\text{is TP}}{=} & 1 - \left(\frac{2^n}{2^n + 1} \right) \sum_{\mathbf{i} \neq \mathbf{0}} \alpha_{\mathbf{i}},
\end{aligned} \tag{71}$$

where in the penultimate line we highlighted that it is the same as for the raw (not-twirled) channel \mathcal{E} , and where we used Eq. (67), with $\mathbf{0}$ being the $2n$ -bit string with all bits being zero, and in the last line the case $\sum_{\mathbf{a}} \alpha_{\mathbf{a}} = 1$ for \mathcal{E} being TP; such expression makes it manifest that average gate fidelity captures only the information of the probability of *any* Pauli error happening¹⁵.

Conversely, the unitarity of the Pauli channel is given by

$$\begin{aligned}
\bar{u}(\mathcal{E}^\odot) &= \frac{\text{tr}[\mathcal{E}^\odot \dagger \mathcal{E}^\odot] - 1}{4^n - 1} \\
&= \frac{\sum_{\mathbf{a}} \lambda_{\mathbf{a}}^2 - 1}{4^n - 1} \\
&= \frac{4^n \sum_{\mathbf{a}} \alpha_{\mathbf{a}}^2 - 1}{4^n - 1},
\end{aligned} \tag{72}$$

which is minimal in the sense that for a non-identity it corresponds to a purely stochastic noise channel, as it only involves the diagonal χ -matrix terms, the Pauli error rates, involved in the average gate-fidelity. Clearly, when the distribution of errors is uniform, i.e., all $\alpha_{\mathbf{i}} = 2^{-n}$ so that the channel is maximally depolarizing, the unitarity vanishes. As opposed to average gate fidelity, the average unitarity of the raw channel \mathcal{E} would capture all elements of its PTM. We can further lower-bound this as follows,

$$\begin{aligned}
\bar{u}(\mathcal{E}^\odot) &= \frac{4^n \sum_{\mathbf{a}} \alpha_{\mathbf{a}}^2 - 1}{4^n - 1} \\
&\leq \frac{4^n \left[\alpha_{\mathbf{0}}^2 + \left(\sum_{\mathbf{b} \neq \mathbf{0}} \alpha_{\mathbf{b}} \right)^2 \right] - 1}{4^n - 1} \\
&\leq \frac{4^n \left[\alpha_{\mathbf{0}}^2 + (1 - \alpha_{\mathbf{0}})^2 \right] - 1}{4^n - 1} \\
&= \left(\frac{2^n \bar{F}(\mathcal{E}) - 1}{2^n - 1} \right)^2 + (4^n - 2) \left(\frac{1 - \bar{F}(\mathcal{E})}{2^n - 1} \right)^2,
\end{aligned} \tag{73}$$

so together with the lower bound $\bar{u} \bar{f}(\mathcal{E})^2$ of [12], we can express the unitarity for the Pauli-twirled channel \mathcal{E}^\odot as

$$\bar{f}(\mathcal{E})^2 \leq \bar{u}(\mathcal{E}^\odot) \leq \bar{f}(\mathcal{E})^2 + \frac{2^{2n} - 2}{(2^n - 1)^2} \bar{r}(\mathcal{E})^2, \tag{74}$$

where here $\bar{f}(\mathcal{E}) = (2^n \bar{F}(\mathcal{E}) - 1)/(2^n - 1)$ is the noise-strength parameter in Eq. (3) in the main text, and $\bar{r}(\mathcal{E}) := 1 - \bar{F}(\mathcal{E})$ is the average gate infidelity of \mathcal{E} .

¹⁵This does *not* mean that average gate fidelity is insensible to coherent errors, but rather that it is only partially so through their contribution to the diagonal elements in the PTM.

The lower bound in Ineq. (74) saturates for depolarizing noise, i.e., when all non-identity Pauli error rates are the same, while the upper bound overestimates the unitarity for Pauli noise through cross-products of non-identity Pauli error rates. Thus, the upper bound serves as a proxy for whether noise has coherent components, if it is above it, or whether it is potentially Pauli, if it is under it.

Of course, in practice, we cannot directly twirl noise quantum channels but we need a way of achieving it by manipulating the noisy gates in question. Whenever the ideal (or target) gates are Clifford, a Pauli twirl can be enforced by a so-called \mathcal{G} -twisted twirl [69], where the outer Pauli operators in Eq. (69) are acted on (or twisted) with the ideal Cliffords. This concept of a twisted-twirl, together with employing random samples instead of all the 4^n possible Pauli operators, are at the core of so-called Randomized Compiling (RC), where we would then effectively have

$$\mathcal{E}_N^\circ(\cdot) := \frac{1}{N} \sum_{P \sim \mathbb{P}_n}^{N \text{ samples}} P \mathcal{E}(P \cdot P) P, \quad (75)$$

where here $P \sim \text{Pauli}$ means P are Pauli samples drawn uniformly at random with no repetition from \mathbb{P}_n , and the sum runs over $N \leq 4^n$ such samples. In practice, this randomized sum would be computed by measuring and then averaging many circuits where the noisy gate is twisted-twirled; considering that the noisy gate may be transpiled into single and two-qubit gates, the way this is usually done is by precisely compiling the single-qubit gates with the Paulis in each random sample, with the overall gate being logically exactly the same. Since also in practice the Pauli operators will be noisy, care has to be taken not to increase the overall number of gates that are executed. In general if the Paulis themselves have coherent noise, perfect diagonalization would be achieved strictly for $N \rightarrow \infty$ by sampling with repetition.

The corresponding PTM of $\mathcal{E}_N^\circ(\cdot)$ has components

$$\begin{aligned} (\mathcal{E}_N^\circ)_{ab} &= \frac{1}{N 2^n} \sum_{\mathbf{q}}^{N \text{ samples}} \sum_{\mathbf{c}, \mathbf{d}} \chi_{cd} \text{tr}[P_{\mathbf{a}} P_{\mathbf{q}} P_{\mathbf{c}} P_{\mathbf{q}} P_{\mathbf{b}} P_{\mathbf{q}} P_{\mathbf{d}} P_{\mathbf{q}}] \\ &= \frac{1}{2^n} \sum_{\mathbf{c}, \mathbf{d}} \left(\frac{1}{N} \sum_{\mathbf{q}}^{N \text{ samples}} (-1)^{\langle \mathbf{q}, \mathbf{c} + \mathbf{d} \rangle} \right) \chi_{cd} \text{tr}[P_{\mathbf{a}} P_{\mathbf{c}} P_{\mathbf{b}} P_{\mathbf{d}}], \end{aligned} \quad (76)$$

where now we can only approximate the property in Eq. (67) with the N random samples of bit strings \mathbf{q} : in the infinite sample limit, $N \rightarrow \infty$, or if exactly each distinct bit string is sampled once, the term within parenthesis goes to δ_{cd} . Since $\langle \mathbf{q}, 2\mathbf{c} \rangle = 0$ for any pair of bit strings \mathbf{q} and \mathbf{c} , the sum over \mathbf{q} when $\mathbf{c} = \mathbf{d}$ equals 1 for any number of samples; this just reflects the fact that twirling (or RC) leaves the diagonal of the PTM invariant. Thus, we can write

$$\begin{aligned} (\mathcal{E}_N^\circ)_{ab} &= \mathcal{E}_{ab}^\circ + \sum_{\mathbf{c} \neq \mathbf{d}} \left(\frac{1}{N} \sum_{\mathbf{q}}^{N \text{ samples}} (-1)^{\langle \mathbf{q}, \mathbf{c} + \mathbf{d} \rangle} \chi_{cd} \frac{\text{tr}[P_{\mathbf{a}} P_{\mathbf{c}} P_{\mathbf{b}} P_{\mathbf{d}}]}{2^n} \right) \\ &:= \mathcal{E}_{ab}^\circ + \frac{1}{N} \sum_{\mathbf{q}}^{N \text{ samples}} \tilde{\lambda}_{ab}^{(\mathbf{q})}, \end{aligned} \quad (77)$$

where here \mathcal{E}° as before, is the perfectly Pauli-twirled channel in Eq. (69), and where we defined

$$\tilde{\lambda}_{ab}^{(\mathbf{q})} := \sum_{\mathbf{c} \neq \mathbf{d}} (-1)^{\langle \mathbf{q}, \mathbf{c} + \mathbf{d} \rangle} \chi_{cd} \frac{\text{tr}[P_{\mathbf{a}} P_{\mathbf{c}} P_{\mathbf{b}} P_{\mathbf{d}}]}{2^n}, \quad (78)$$

which correspond to the off-diagonal elements of the PTM upon the twirl action of an element $P_{\mathbf{q}}$. The effect of $N = 1$, a single randomization, will simply be to either change a sign of an off-diagonal element or leave it as it is. For an even number N of samples, the off-diagonals will either vanish or

be suppressed in magnitude as integer multiples of $2/N$ (with ratio less than one). On the other hand, for odd N , all off-diagonals vanish in magnitude as integer multiples of $1/N$.

Finally, then

$$\bar{u}(\mathcal{E}_N^{\mathcal{O}}) = \bar{u}(\mathcal{E}^{\mathcal{O}}) + \frac{1}{N^2} \sum_{\mathbf{q}, \mathbf{q}'}^{N \text{ samples}} \frac{\tilde{\lambda}_{\mathbf{ab}}^{(\mathbf{q})} \tilde{\lambda}_{\mathbf{ba}}^{(\mathbf{q}')}}{4^n - 1}, \quad (79)$$

where similarly now, the off-diagonal contributions will vanish as (small) multiples of $1/N^2$.